Master´s Thesis

Master in Neuroengineering and Rehabilitation (MUNR)

Characterising brain connectivity along the lifespan in a rodent model of healthy ageing

REPORT

July 1, 2023

Author: Elena Espinós Soler

Supervisor: Silvia De Santis

Co-supervisor: Alejandro Bachiller Matarranz

Semester: 06/2023

ETSEIB

Escola Tècnica Superior
d'Enginyeria Industrial de Barcelona

UPC

Abstract

The brain parenchyma undergoes several structural changes throughout life, which have a major impact on its physiological evolution, and which are behaviorally reflected as changes in cognition and ability. A key question is how age-related structural alterations impact the function of the different areas. Functional connectivity, measured as correlation between brain regions during the resting state Magnetic Resonance Imaging (MRI), is a quantitative measure of function that can be reliably used to characterize the evolution of the communication between regions across the lifespan. However, most of the works so far have done it with a hypothesis driven approach. The present work aims to identify the functional connectivity patterns of the whole brain during resting state in a rodent model of healthy ageing. For this purpose, we have followed the standard workflow recently proposed in a consensus paper on functional imaging processing in preclinical MRI. We have set up a longitudinal functional MRI experiment to measure functional connectivity in rats at different times. Independent component analysis has been used to identify characteristic resting-state networks and compare them between three different ages, corresponding to adulthood to early senescence. The goal is to highlight region-, sex-, and age-specific patterns that drive the physiological decline in cognition observed in senescence, with potential to identify vulnerable regions in and define targets for intervention. Our results uncovered patterns of increased functional connectivity between adulthood and senescence in several key regions controlling the functions known to be affected by age. Such increase in connectivity can be explained as a compensatory mechanism that allows the brain to cope with reduced microstructural integrity. The study of healthy ageing in absence of disease sets the baseline for the identification of pathological conditions.

Keywords: MRI, BOLD, fMRI, rs-fMRI, functional connectivity, ICA, ageing, longitudinal, rat.

Resumen

El parénquima cerebral experimenta varios cambios estructurales a lo largo de la vida, que tienen un gran impacto en su evolución fisiológica, y que se reflejan conductualmente como cambios en la cognición y la capacidad. Una cuestión clave es cómo repercuten las alteraciones estructurales relacionadas con la edad en la función de las distintas áreas. La conectividad funcional, medida como correlación entre regiones cerebrales durante la Resonancia Magnética (RM) en estado de reposo, es una medida cuantitativa de la función que puede utilizarse de forma fiable para caracterizar la evolución de la comunicación entre regiones a lo largo de la vida. Sin embargo, la mayoría de los trabajos realizados hasta ahora lo han hecho con un enfoque basado en hipótesis. El presente trabajo pretende identificar los patrones de conectividad funcional de todo el cerebro durante el estado de reposo en un modelo de roedor de envejecimiento sano. Para ello, hemos seguido el flujo de trabajo estándar propuesto recientemente en un documento de consenso sobre el procesamiento de imágenes funcionales en RM preclínica. Hemos establecido un experimento de RM funcional longitudinal para medir la conectividad funcional en ratas en diferentes momentos. Se ha utilizado el análisis de componentes independientes para identificar redes características en estado de reposo y compararlas entre tres edades diferentes, correspondientes a la edad adulta y a la senescencia temprana. El objetivo es destacar los patrones específicos de región, sexo y edad que impulsan el declive fisiológico de la cognición observado en la senescencia, con potencial para identificar regiones vulnerables y definir objetivos de intervención. Nuestros resultados descubrieron patrones de aumento de la conectividad funcional entre la edad adulta y la senescencia en varias regiones clave que controlan las funciones que se sabe que se ven afectadas por la edad. Este aumento de la conectividad puede explicarse como un mecanismo compensatorio que permite al cerebro hacer frente a la reducción de la integridad microestructural. El estudio del envejecimiento sano en ausencia de enfermedad sienta las bases para la identificación de condiciones patológicas.

Palabras clave: MRI, BOLD, fMRI, rs-fMRI, conectividad funcional, ICA, envejecimiento, longitudinal, rata.

Resum

El parènquima cerebral experimenta diversos canvis estructurals al llarg de la vida, que tenen un gran impacte en la seua evolució fisiològica, i que es reflecteixen conductualment com a canvis en la cognició i la capacitat. Una qüestió clau és com repercuteixen les alteracions estructurals relacionades amb l'edat en la funció de les diferents àrees. La connectivitat funcional, mesurada com a correlació entre regions cerebrals durant la Ressonància Magnètica (RM) en estat de repòs, és una mesura quantitativa de la funció que pot utilitzar-se de manera fiable per a caracteritzar l'evolució de la comunicació entre regions al llarg de la vida. No obstant això, la majoria dels treballs realitzats fins ara ho han fet amb un enfocament basat en hipòtesi. El present treball pretén identificar els patrons de connectivitat funcional de tot el cervell durant l'estat de repòs en un model de rosegador d'envelliment sa. Per a això, hem seguit el flux de treball estàndard proposat recentment en un document de consens sobre el processament d'imatges funcionals en RM preclínica. Hem establit un experiment de RM funcional longitudinal per a mesurar la connectivitat funcional en rates en diferents moments. S'ha utilitzat l'anàlisi de components independents per a identificar xarxes característiques en estat de repòs i comparar-les entre tres edats diferents, corresponents a l'edat adulta i a la senescència primerenca. L'objectiu és destacar els patrons específics de regió, sexe i edat que impulsen el declivi fisiològic de la cognició observat en la senescència, amb potencial per a identificar regions vulnerables i definir objectius d'intervenció. Els nostres resultats van descobrir patrons d'augment de la connectivitat funcional entre l'edat adulta i la senescència en diverses regions clau que controlen les funcions que se sap que es veuen afectades per l'edat. Aquest augment de la connectivitat pot explicar-se com un mecanisme compensatori que permet al cervell fer front a la reducció de la integritat microestructural. L'estudi de l'envelliment sa en absència de malaltia estableix les bases per a la identificació de condicions patològiques.

Palabras clave: MRI, BOLD, fMRI, rs-fMRI, connectivitat funcional, ICA, envelliment, longitudinal, rata.

Contents

Acronyms

AFNI	Analysis of Functional NeuroImages.
ANTs	Advanced Normalization Tools.
bf	Barrel field.
BIDS	Brain Imaging Data Structure.
BOLD	Blood-oxygen-level-dependent.
CoBra Lab	Computational Brain Anatomy Laboratory.
CPU	Central Processing Unit.
CSF	Cerebrospinal fluid.
CSIC	Consejo Superior de Investigaciones Científicas.
DMN	Default Mode Network.
dMRI	Diffusion MRI.
EPI	Echo planar Imaging.
FC	Functional connectivity.
fMRI	Functional Magnetic Resonance Imaging.
FOV	Field of view.
FSL	FMRIB Software Library.
GB	Gigabyte.
GLM	Generalized Linear Model.
GM	Grey matter.
ICA	Independent Component Analysis.
ISMRM	International Society for Magnetic Resonance in Medicine.
ITK	Insight Toolkit.
MCFLIRT	Motion Correction using FMRIB's Linear Image Registration Tool.
MELODIC	Multivariate Exploratory Linear Optimized Decomposition into Independent Components.
MR	Magnetic Resonance.
MRI	Magnetic Resonance Imaging.
NMR	Nuclear Magnetic Resonance.
PICA	Probabilistic ICA.
RABIES	Rodent Automated Bold Improvement of EPI Sequences.

RAM	Random Access Memory.
RARE	Rapid Acquisition with Refocusing Echoes.
rs-fMRI	Resting-state functional Magnetic Resonance Imaging.
RSN	Resting State Networks.
SAMRI	Small Animal Magnetic Resonance Imaging.
STAC	The Scaffolding Theory of Aging and Cognition.
T	Tesla.
TE	Time to Echo.
TR	Repetition Time.
WM	White matter.

List of Figures

List of Tables

1 Preface

1.1 Origin of the Project

The project is a collaboration with Instituto de Neurociencias de Alicante (Consejo Superior de Investigaciones Científicas (CSIC) and Miguel Hernandez University of Elche) in the Translational Imaging Biomarkers laboratory[1]. Its research focuses on the development, optimization and application of innovative, non-invasive and translational magnetic resonance imaging tools. For this purpose, Resting-state functional Magnetic Resonance Imaging (rs-fMRI) data acquired at the institute were used in order to study the changes in brain connectivity during healthy ageing in rodent models.

1.2 Motivation

Animal research in neuroscience is fundamental to characterize both healthy and pathological trajectories of brain structure and function, providing important information inaccessible in humans.

The ease of breeding and reproduction, its small size and the ability to be genetically manipulated, make rodents a popular choice in neuroscience research. Although translating the results of studies in animal models to humans can be a complex process and not always direct, there are several reasons for doing so. In this case, the aim is to characterize brain evolution using Magnetic Resonance Imaging (MRI), a technique easily translatable to humans and suitable for studies in vivo. In addition, ageing studies in rodents are ideal due to the shorter lifespan, which allows longitudinal analyses.

1.3 Previous requirements

The requirements for the development of this project are, on the technical side:

- Hardware: 32GB RAM and 16-core CPU system (as a minimum).
- Software: FSL[2], AFNI[3], Nipype[4], ANTs[5], MATLAB & ITK-Snap[6]

Additionally, in order to be able to carry out the study it is necessary:

- Knowledge in neuroimaging processing.
- Knowledge in the different modalities of magnetic resonance imaging.
- Knowledge of the tools and libraries necessary for data processing
- Knowledge in rodent models for neuroimaging studies.

[1] https://in.umh-csic.es/es/grupos/biomarcadores-de-imaging-translacional/
[2] https://fsl.fmrib.ox.ac.uk/fsl/fslwiki/FSL
[3] https://afni.nimh.nih.gov/
[4] https://nipype.readthedocs.io/en/latest/#
[5] http://stnava.github.io/ANTs/
[6] http://www.itksnap.org/pmwiki/pmwiki.php?n=Main.HomePage

2 Introduction

2.1 MRI

Thanks to its versatility, Magnetic Resonance Imaging (MRI) provides access to information on brain anatomical structure, neuronal connections and their activation in a non-invasive fashion. Such information can be used to highlight alterations in pathological conditions, but also characterize trends of specific aspects of brain structure and function during maturation and ageing.

MRI employs electromagnetic radiation on a sample exposed to a strong magnetic field. It is based on the ability of protons to resonate under an external magnetic field (B_o) known as Nuclear Magnetic Resonance (NMR). In this resonance state, the protons are able to absorb energy when a radiofrequency pulse is applied, and release it when the stimulation is off. This energy emission will be different depending on the environment surrounding the protons, which gives information about the composition of the tissue (White matter (WM), Grey matter (GM) or Cerebrospinal fluid (CSF)), but also on its location inside the scanner, allowing images of the whole brain to be reconstructed.

A radio frequency (RF) pulse is applied in a plane perpendicular to the magnetic field, known as transverse magnetisation, and causes the hydrogen nuclei to deviate their longitudinal magnetisation and rotate around the magnetic field. When the RF pulse stops, the hydrogen nuclei begin to relax and return to their original longitudinal magnetisation state. During this process, the hydrogen nuclei emit a signal dependent on several factors, such as the applied magnetic field, the frequency and duration of the RF pulse, and the relaxation properties of the body's tissues. The relaxation time is the time to return to magnetization equilibrium. Relaxation combines two mechanisms: longitudinal relaxation and transversal relaxation. The relaxation time T1 or longitudinal relaxation time defines the time taken by the net magnetization M returns to its initial maximum value M_o parallel to the magnetic field B_o [1]. The relaxation time T2, also known as transversal relaxation time or spin-spin, is the time required for the transverse magnetization to fall to approximately 37% of its initial value [2].

By applying magnetic field gradients in addition to the B_o, it is possible to localize spatially the origin of the signal; in this way, 3D images can be reconstructed. The anatomical details in the image depend on how the hydrogen nuclei in different body tissues respond to the mag-

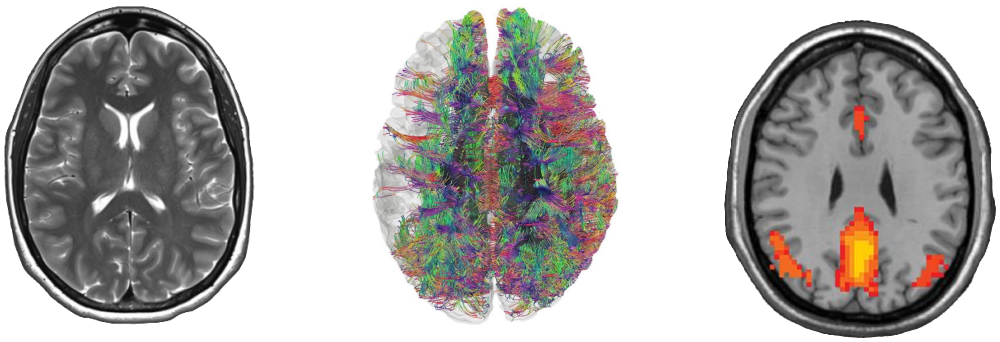

(a) T2*-weighted imaging (b) Diffusion MRI (c) Functional MRI

Figure 1: **Main modalities of MRI.**

netic field and the RF pulse. For example, tissues with more water, such as the brain, generate stronger signals than tissues with less water, such as bone [3].

There are different MRI modalities but the three main ones are: structural, diffusion and functional imaging (figure 1). Structural imaging provides anatomical structures information. Diffusion MRI (dMRI) or Diffusion-weighted imaging provides microstructural and anatomical connectivity information. Functional imaging or Functional Magnetic Resonance Imaging (fMRI), provides information about brain neurons activity, in response to an specific stimuli or task (task fMRI) or in relation to the spontaneous activity of the neurons (Resting-state functional Magnetic Resonance Imaging (rs-fMRI)).

The combination of different modalities allows counteracting the limitations presented by each of them separately, such as low spatial resolution in fMRI compared to better spatial resolution in structural MRI but with longer acquisition time for a single volume, for example. Multimodality eniches the information extracted by an MRI experiment, allowing to boost both specificity and sensitivity[3].

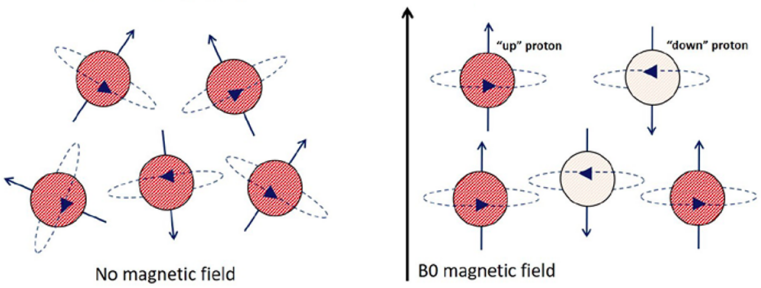

(a) Protons in the body (b) Protons in MRI scanner

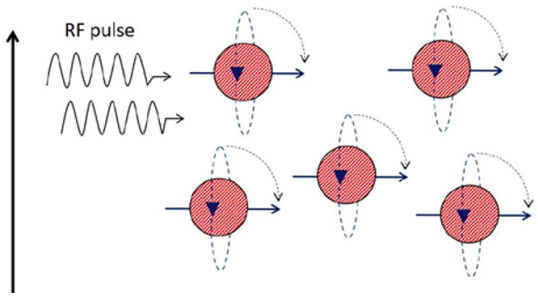

(c) Protons with a RF pulse

Figure 2: **Behaviour of hydrogen protons. Image adapted from [69]**

2.1.1 fMRI

Functional Magnetic Resonance Imaging (fMRI) is a non-invasive neuroimaging tool that measures small changes in blood flow (the hemodynamics) due to brain activity. The communication between neurons requires energy provided in the form of oxygen and glucose. When neurons are activated, they trigger a cascade of biochemical and metabolic events in the brain involving oxygen consumption. In order for neurons to receive the oxygenated blood supply in response to increased neuronal activity, blood flow and local cerebral blood volume are in-

creased. This also means that the concentration of oxygenated hemoglobin increases in areas of increased neuronal activity and this disturbs the local magnetic field (B_o). Specifically, the local magnetic field (B_o) in the presence of deoxyhemoglobin becomes less uniform which leads to a reduction of the signal of water molecules in the region. These changes in the magnetic resonance signal are known as the Blood-oxygen-level-dependent (BOLD) effect.

fMRI relies upon the quantification of the Blood-oxygen-level-dependent (BOLD) effect through T2* relaxation: slower T2 attenuation indicates activity.

2.1.2 Resting State fMRI

While fMRI can be used to highlight structures that gets activated during a task, the brain also possess an intrinsic activity when at rest. This phenomenon can be quantified by rs-fMRI.

Functional connectivity (FC) can be defined as the temporal correlation between two BOLD signals at very low frequencies (<0.1Hz) from different parts of the brain. The similarity of these may indicate that the regions are communicating. It should be noted that this functional relationship does not indicate directionality. Given two related regions, we cannot interpret that one region is responsible for the activity in the other [4, 5].

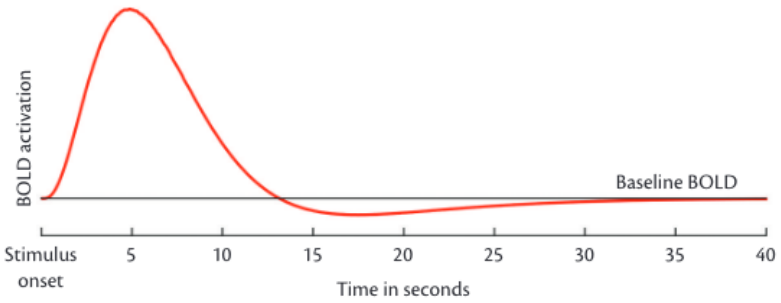

Figure 3: **Hemodynamic response function representation.**

This intrinsic activity is a relatively slow process that peaks at approximately 5-6 seconds after the onset of neuronal activity as shown in figure 3.

2.1.3 Resting State Networks

The similarity of two BOLD signals is quantified by observing temporal correlation maps. The brain regions that have similar patterns of oscillation during the resting state are called Resting State Networks (RSN). By grouping regions on the basis of their similarity in the BOLD signal fluctuations, several networks consistently emerge both in humans and rodents, the most prominent being the Default Mode Network (DMN) (figure 4). This network is characterized by being active at rest and inactive during cognitive tasks. This network is related with several cognitive processes such as episodic memory, self-referential processing and mind wandering [6].

Two other networks of interest in humans are the salience and the executive control network (ECN). ECN network is engaged in cognitively demanding tasks, such as decision-making and working memory. Salience is involved in evaluating the relevance of internal and external stimuli in order to generate appropriate responses [7].

Other networks can also be identified, both in humans and rats, such as the visual network,

primary somatosensory network, auditory and dorsal attention among others [66]. In rodents it is possible to find RSN such as those shown in the figure 8.

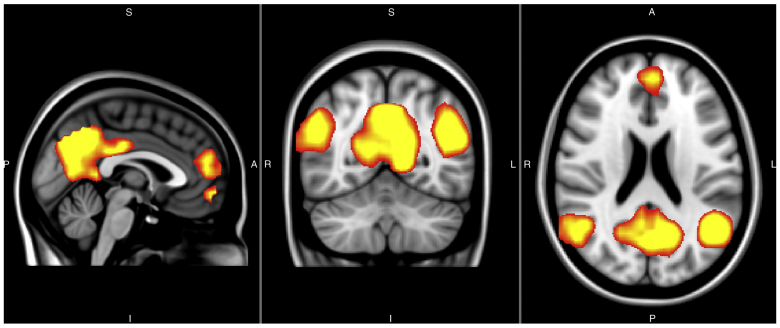

Figure 4: **Default mode network (DMN)**. Brain structures active during resting state. Image extracted from [8]

2.2 Ageing

Ageing is the primary risk factor for most neurodegenerative diseases, including Alzheimer's disease (AD) and Parkinson disease (PD) [9]. Throughout the lifespan, the brain experiences numerous microstructural and functional alterations that significantly impact its physiological and cognitive evolution. It is important to characterize the patterns of both healthy development and deterioration in order to comprehend the factors contributing to a healthy aging process and establish a reference point for identifying pathological conditions.

Characterizing brain evolution as we age, is crucial to uncover the factors that contribute to a healthy aging process. This information also lays the foundation for comprehending aging as a risk factor for illnesses. Hence, it is imperative to establish and describe specific, non-invasive indicators of brain health throughout one's lifetime, which have the possibility of enhancing current methods of diagnosis and monitoring treatment effectiveness [10, 11]. It's important to take into account the relationship between aging and the structural, neurochemical changes, cell proliferation, synaptogenesis and myelination, as well as differential immune responses seen at different ages and its impact in cognition [12].

Aging is accompanied by cognitive deficits in areas such as episodic and working memory (ability to retain and manipulate short-term information) and executive control. The speed at which we process information is also reduced with age. Ageing affects cognitive flexibility and inhibits automatic responses[13, 14]. The cognitive consequences may be due to changes in different brain areas. For example, the frontal-striatal and medial frontal areas influence the capacity for attention and working memory. Also, in the face of a reduction in these capacities, increased recruitment in frontal areas is observed as a form of compensation [15]. On the other hand, the retrosplenial cortex acts as an interface between the working memory functions enabled by the prefrontal cortex and the long-term memory functions supported by the medial temporal lobe memory system. Memory dysfunction in aging may be related to the disruption of the functioning of connected cortical networks, including the retrosplenial cortex. Cognitive memory deficits are also due to reduced connectivity in posterior cortical areas [14].

Despite differences between the two species, it is worth to study the evolution of the brain parenchyma over time both in rodents, as a model for human ageing. The advantage is that the time scale between these two species is quite different (figure 6) but the sequence of key

events in brain maturation coincides to a large extent [12]. It is important to note that aging affects each individual uniquely, and cognitive changes may vary in their magnitude and rate of progression. Superagers, for example, are individuals aged 80 years or older who pass tests of memory, attention and other cognitive skills at levels comparable to adults decades younger [16].

2.2.1 Functional differences with sex-perspective

As mentioned above, the study of aging is important to identify which factors contribute to this process, but it is also important to take into account the sex perspective. Characterizing sex-specific trajectories of healthy ageing is important to understand the different susceptibility of male and females to many age-related brain pathologies.

Different research studies report the results of how different tests and trials help to characterize these cognitive and functional connectivity differences both in humans and rodents but also there are many others that do not reproduce these differences that others mention [17].

Figure 5 shows the trajectory of different cognitive functions with aging according to sex. In general, in early and middle adulthood, women have better verbal and episodic memory [18, 19] while men have better spatial memory. Furthermore, females tend to exhibit higher initial performance on tasks involving global cognition and executive functioning. However, as they age, women tend to experience a more pronounced decline in their performance compared to men [20]. In both sexes, with aging, cognitive processing speed is reduced and is more pronounced in men than in women, which means that women can maintain a relatively better processing speed with age [21, 22].

The fact that there are cognitive and developmental differences between sexes or that the prevalence of certain diseases is different is attributed to hormonal, genetic and socioeconomic factors. Differences between sexes are observed as early as childhood due to hormonal changes caused by puberty and later by menopause.

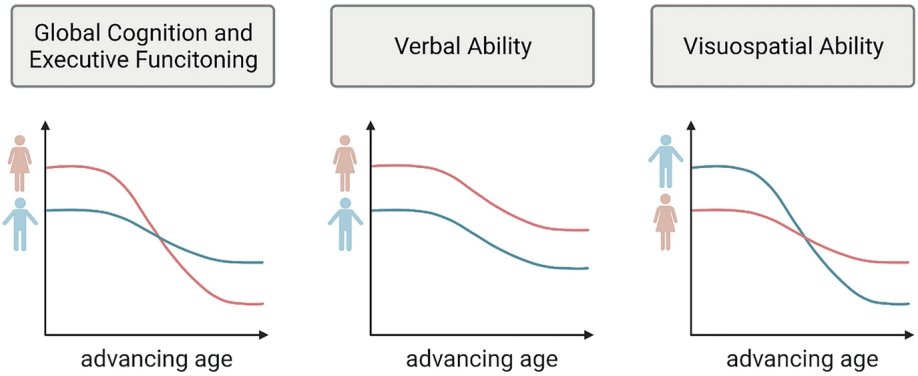

Figure 5: **Sex differences in the trajectory of cognitive aging across different domains.** Image obtained from [23]

2.3 fMRI processing - State of the art

Rodents have become a valuable model for investigating healthy aging in research studies using MRI. These animals are ideal for studying longitudinal age-related changes in the brain due to the biological and physiological similarities with humans and their short life expectancy (2-3

years) and after translate findings across species. Rats and mice are commonly used in laboratory research although, only a few longitudinal imaging studies are available such as Fowler et al. [24] or Bellantuono et al. [25].

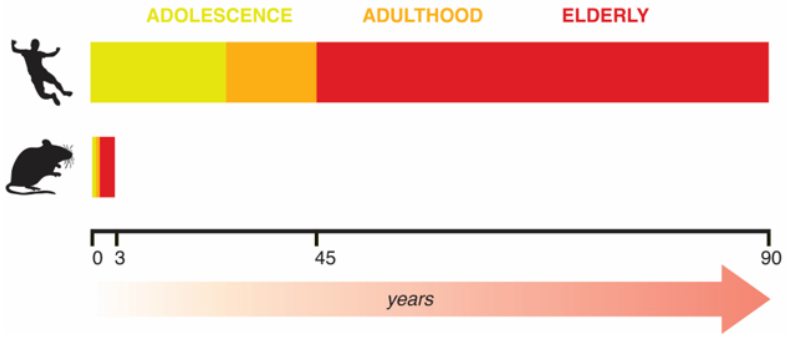

Figure 6: **Development stages in animal and human model.**

The state of the art focuses on what are the current objectives in the study of fMRI: research teams work on improving and optimizing resources and unifying them so that the processing and interpretation of results is reproducible and robust.
Current tools such as SAMRI[7] or RABIES[26], an opensource pipeline created by researchers at Computational Brain Anatomy Laboratory (CoBra Lab), allow the preprocessing and subsequent analysis of fMRI data in rodents. These pipelines make use of tools such as FSL, nibabel, ANTs, among others and **their goal is to promote interoperability and cooperation.**

Figure 7 shows the pipeline defined by RABIES, a rat fMRI acquisition protocol with optimized acquisition and processing parameters, a reproducible pipeline for data acquired with diverse protocols and determined experimental and processing parameters associated with the robust detection of Functional connectivity (FC). It is included in StandarRat, a consensus by Grandjean J. et al.[27]. They showed that an standardized protocol enhances biologically plausible FC patterns relative to previous acquisitions.

In addition, it is important to highlight that *"the issue of confound correction for resting-state fMRI remains largely unresolved among human literature, and is only beginning to be studied in rodents"*[27]. This is a constantly evolving field of great importance in fMRI processing and in case of fMRI correction in humans as they mentioned, in Wang, Hao-Ting, et al.[28], they propose a new benchmark using the fMRIPrep[8] pipeline and Nilearn.

In conclusion, efforts to improve and unify fMRI processing tools in animal models allow for better interpretation and reproducibility of results. Also, the use of rodents in MRI studies of healthy aging offers a valuable tool for gaining a deeper understanding of the underlying mechanisms of aging and developing new treatments to improve health and quality of life in old age.

[7] Small Animal Magnetic Resonance Imaging https://github.com/IBT-FMI/SAMRI
[8] Robust Preprocessing Pipeline for fMRI Data https://fmriprep.org/en/stable/

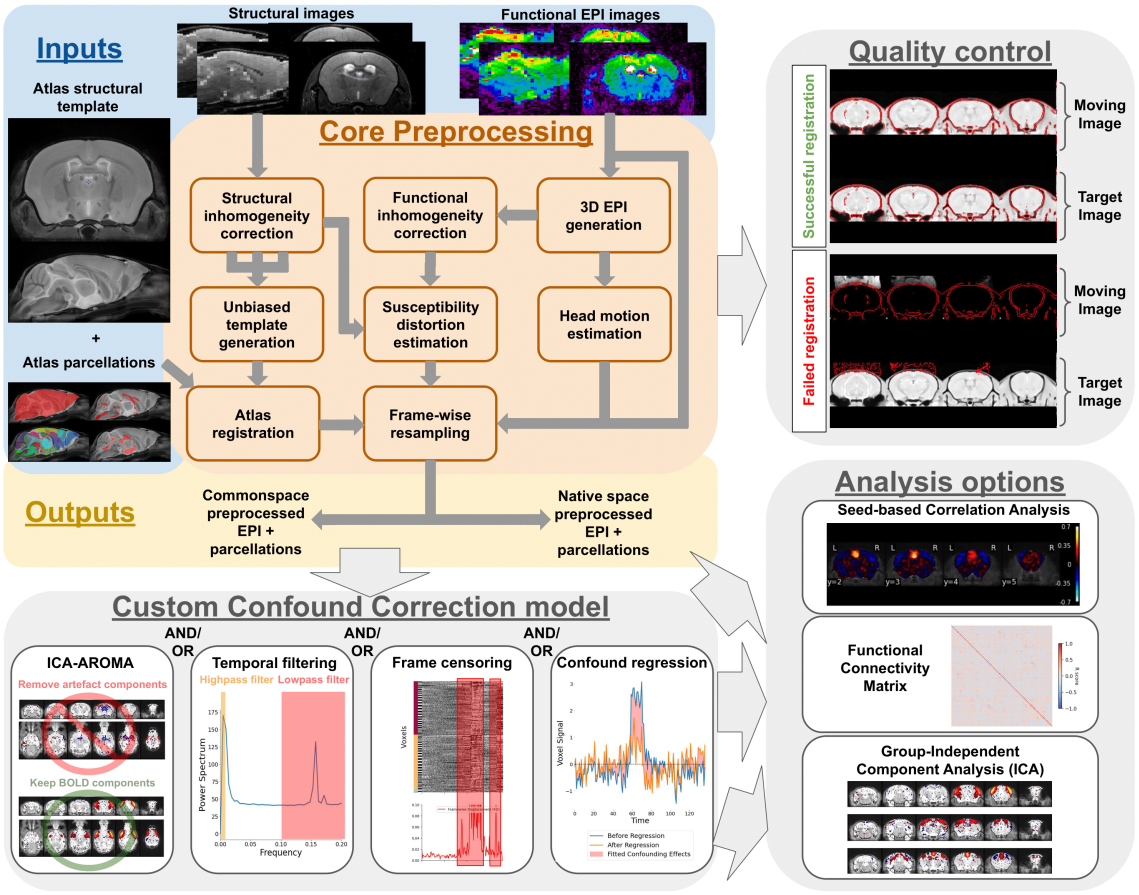

Figure 7: **RABIES pipeline schema.**

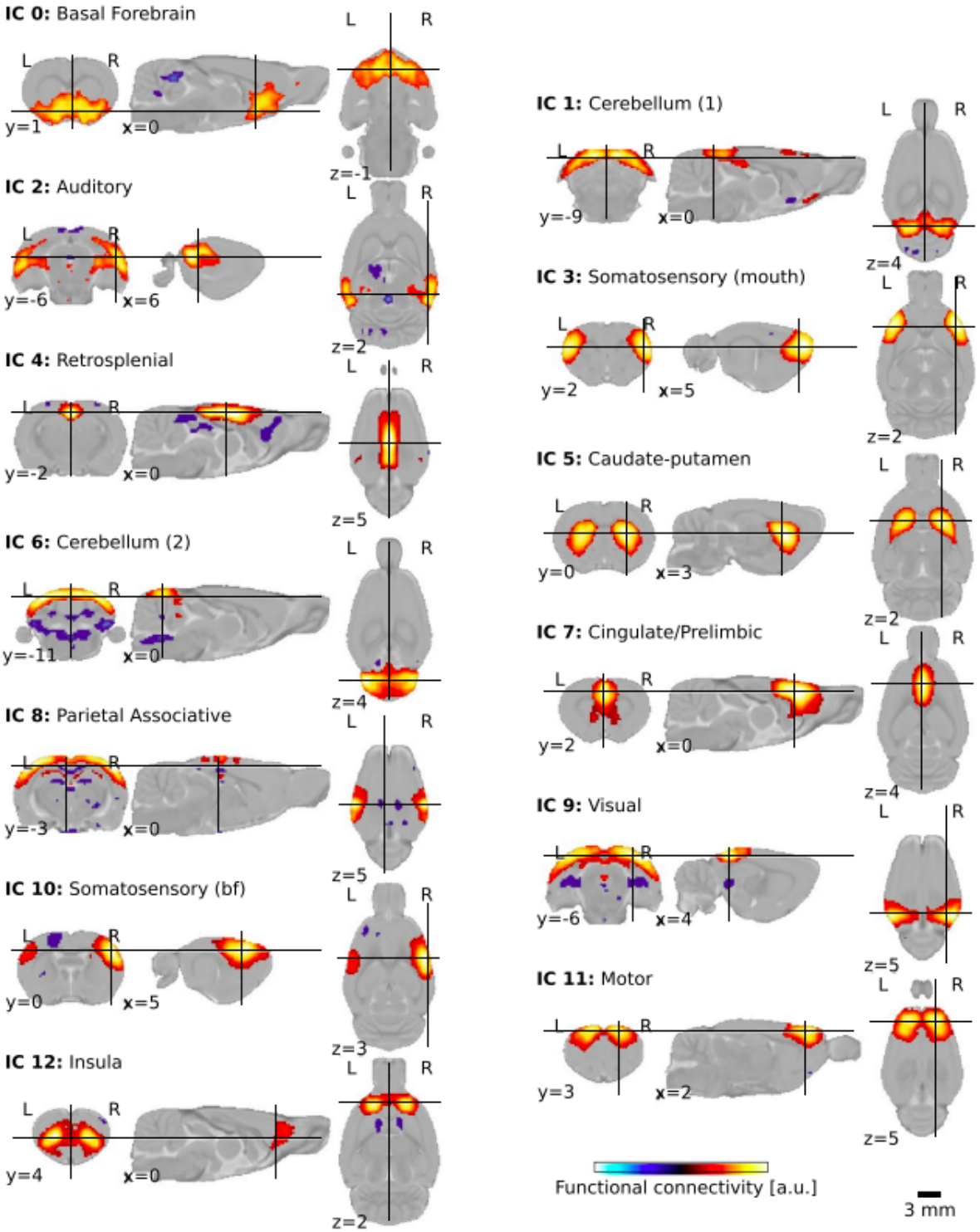

Figure 8: **Resting state network maps in rodents.** Image extracted from [27]

3 Objectives

Based on the introduction and the state of the art of the work, the main objective of this project is ***to investigate the brain functional connectivity in a longitudinal rat model of healthy aging using resting-state functional MRI***. This longitudinal aging study is carried out by acquiring fmri sequences on a wild type rat animal model and including both sexes.

The secondary objectives of the study are:

- **Obj. 1** Develop a functional magnetic resonance image preprocessing and analysis pipeline for preclinical data including state-of-the-art analysis tools.
- **Obj. 2** To identify the brain anatomical correlates of functional organization longitudinally in a rat model of healthy ageing.
- **Obj. 3** To interrogate significant effects of age on brain networks connectivity.
- **Obj. 4** To understand functional brain differences between sexes because of ageing.

4 Materials and methods

4.1 Animals

The analysed cohort was composed by female and male Wistar rats, exhamined at 210, 364 and 546 postnatal-days. Since not all rats completed the study and some images were removed due to unsufficient quality, at the first timepoint the sample size was 7 females and 7 male rats; at 364 days, 8 females and 8 males and on day 546, MRIs were acquired from 5 females and 4 males.

4.2 Data acquisition

MR images were acquired on a 7T (Tesla) small animal MRI scanner (Bruker, BioSpect 70/30). Although the aim of this protocol involves functional images, anatomical and functional data are needed.

For fMRI, an Echo planar Imaging (EPI) sequence (figure 9b) were acquired with a TE[9] = 15 ms, a TR[10] = 2000 ms, Field of view (FOV) of 25×25 mm^2, a matrix of 50x50, fifty-six slices covering the whole brain with a FOV of 25×25 mm^2 and a matrix size of 50 x 50, in plane resolution 0.5×0.5 mm^2, a slice thickness of 0.5 mm and a total of 600 volumes. Anatomical MRI data (figure 9a) were acquired using a RARE sequence with factor 8; a matrix size of 200 × 200 and fifty-six slices that covered the whole rat brain with a plain resolution of 125 x 125 x 500 μm^3 , a Field of view (FOV) of 25×25 mm^2, a TR=6253 ms and TE=11 ms and 4 averages.

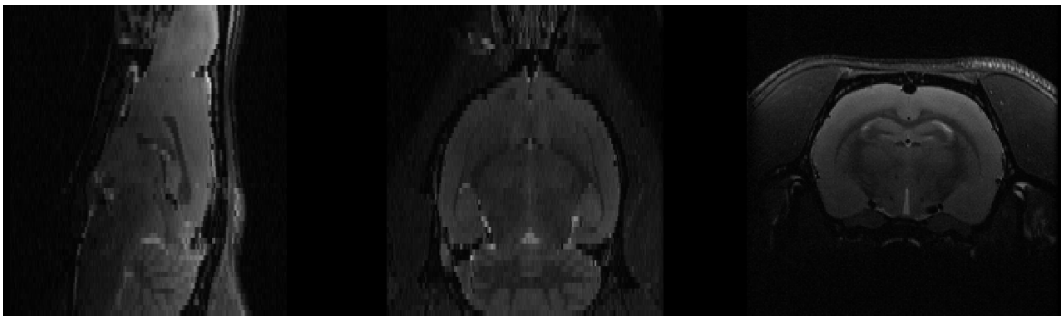

(a) T2w MRI sequence.

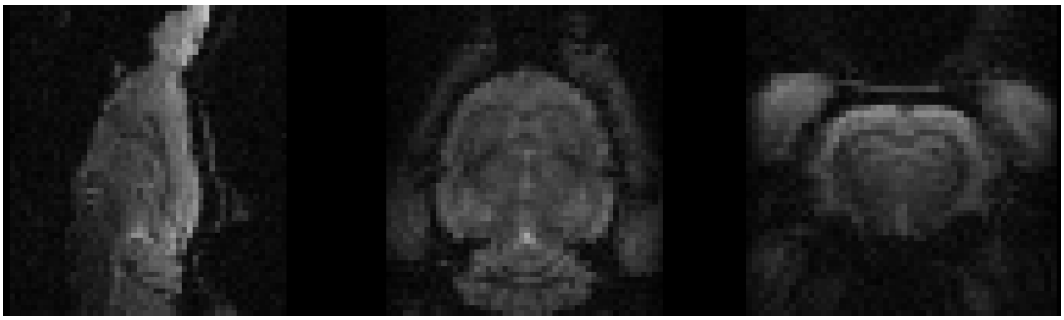

(b) Echo planar Imaging (EPI) MRI sequence.

Figure 9: **Anatomical and functional sequences acquired in the study.** Sagittal (left), horizontal (middle) and coronal (right) planes.

[9] Time to Echo (TE) is the time between the delivery of the RF pulse and the receipt of the echo signal.
[10] Repetition Rime (TR) is the time between successive pulse sequences applied to the same slice.

4.3 Anesthetics

During the acquisition of the sequence in animals the use of anesthesia is required to prevent movement and relieve stress on the animal. In this acquisition protocol isoflurane/O_2 5% (vol/vol) has been used for anesthesia induction. During the anatomical sequence acquisition the anesthesia was maintained at 2% (vol/vol) and for rs-fMRI it was reduced to 1.5% (vol/vol).

4.4 Data preprocessing

To carry out the analysis of the RSNs, the procedure is divided into two main blocks: **(I) Data Preprocessing** and **(II) Brain Network Analysis**. The first block details the **(Data preparation, Anatomical preprocessing and Functional preprocessing**. This data processing is carried out at the subject-level while the second block, the Brain Network Analysis, is a group-level analysis. Most of the pre-processing has been carried out with the tools provided by FSL, AFNI, ANTs, ITKSnap and the Nipype Python library. All the steps followed during the development are described in detail and in order as follows. It is important to note that for an optimal processing of the functional images, it is necessary to work previously with the structural MRI, which has a higher spatial resolution.

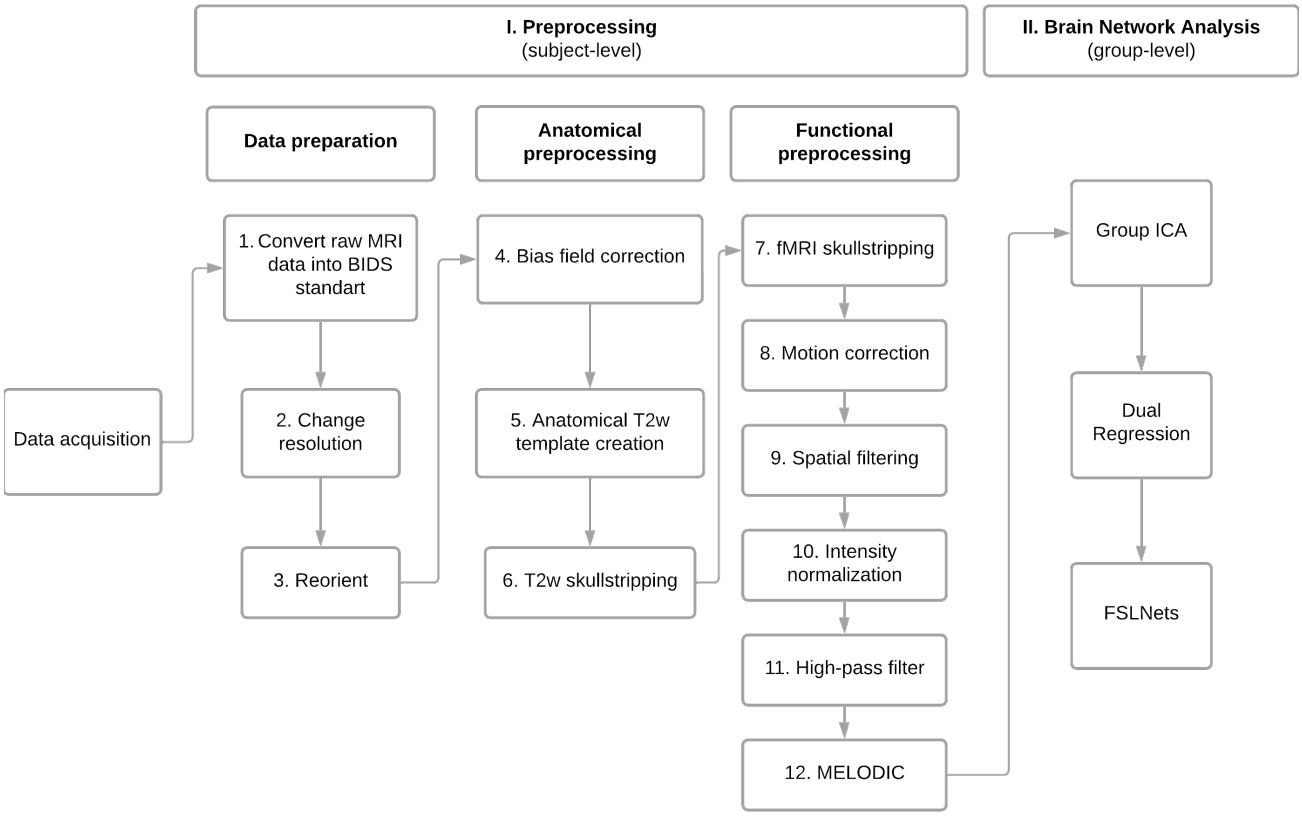

Figure 10: **Pipeline to preprocess and analyse fMRI data.**

The following sections will describe in detail each of the steps followed in the processing and analysis of the data.

4.4.1 Data preparation

Step 1. Convert Raw data into Nifti format. The acquired images are in the Bruker software's native output format. Thus, the first step is to convert the raw data into Nifti format. For that, the Bruker-ParaVision MRI to Nifti format tool, Bru2Nii[11], is used. Once the conversion was done, the files were renamed and structured following the Brain Imaging Data Structure (BIDS)[12] standard.

Step 2. Change of the resolution. The majority of MRI tools have been designed for humans (e.g. FSL tools), therefore, the dimensions and orientations of the images are different. Since we are working with rodent MRIs, it is necessary to increase them by a factor of 10 so that they are comparable to human voxel size. Code 1 shows how to augment the resolution of a nifti image using Python.

Listing 1: Python code to change the nifti image resolution.

```
img = nib.load(img)
header = img.header # get the header

# create a copy
qformcode = header['qform_code'].copy()
sformcode = header['sform_code'].copy()

# change the sform and the qform
# augmenting pixidm = will change the qform
header['pixdim'][1:4] = header['pixdim'][1:4] * factor

# augmenting the affine = will change the sform
img.affine[0][0] = img.affine[0][0] * factor
img.affine[2][1] = img.affine[2][1] * factor
img.affine[1][2] = img.affine[1][2] * factor

# create a new image using the matrix values, affine matrix & header
new_img = nib.Nifti1Image(values, img.affine, header)

nib.save(new_img, output_name) # save augmented image
```

Step 3. Modify the orientation. The orientation of the head when the animal is introduced in the resonance is different from the reference orientation in humans and also the type of coil used during the acquisition changes the resulting image. With the command:

$$\textbf{\textit{fslswapdim}} < hdrfile > xyz < hdrfile\_flip >$$

we reorient the image following the axis left-right, anterior-posterior and superior-inferior, according to the standard. This command only rotates and flips the images on the three axes. The parameters x,y and z represents the spatial coordinates from left to right, from front to back and from bottom to top respectively[13].

Another possible way to modify manually the orientation of the image according to the human reference system is to access the header metadata. As the FSL program uses the sform matrix to represent the image position and orientation in space, the image is reoriented by modifying the matrix elements.

[11] https://github.com/neurolabusc/Bru2Nii
[12] https://bids.neuroimaging.io/
[13] https://fsl.fmrib.ox.ac.uk/fsl/fslwiki/Orientation%20Explained

4.4.2 Anatomical preprocessing

Step 4. Bias field correction. During the acquisition of both anatomical and functional sequences, artifacts such as inhomogeneities in the field or the movement of the animal distort the signal. To correct the low frequency intensity non-uniformities that appear during the acquisition of the sequence, a SimpleITK algorithm, *N4BiasFieldCorrection*, is applied to the anatomical images. It uses a nonparametric approach to estimate and correct for field bias in MRI images. The method is based on the assumption that signal inhomogeneity can be modeled as a smooth multiplicative bias field. The tool uses local information from the image to estimate this bias field and then applies it to correct the original image.

Step 5. Anatomical template creation. When all the images are in the correct dimensions and orientations, we proceed to obtain an anatomical template of the set of subjects of the experiment. The template is needed because with it, it is possible to obtain the brain extraction of all the subjects of the study. Also, for the later Independent Component Analysis (ICA) of the functional images, this template is used as a standard space for all of them.
For this purpose *buildtemplateparallel.sh*, an open source ANTs tool has been used. The obtained outputs are the anatomical template and the *Affine*, *Warp* and *InverseWarp* files of each subject individually. The *Affine* and *Warp* files are the result of a direct, linear and non-linear transformation respectively, that is used to deform the image in moving space (native space) and produce an output in fixed space (common space).

In another case in which an anatomical template is already available, each of the individual anatomical images should be registered on it by the function *antsRegistrationSyN.sh*[14] as follows, for example.

antsRegistrationSyN.sh *-d 3 -f fixedImg.nii -m movingImg.nii -o movingToFixed -t s*

The algorithm implements a technique called "Synthetic Diffusive Registration" (SyN), which is a nonlinear registration method based on deformation fields. It works by finding a non-rigid transformation that maps a source image to a target image. To achieve this, the algorithm uses a combination of similarity measures between the images and optimization methods to find the optimal deformation parameters. The result of this algorithm returns the registered image, the deformation field, the linear transformation and the registration metrics.

Step 6. Skullstripping. From the anatomical template, the mask of the brain is obtained, which allows to segment the brain signal from the rest (figure 11). The FSL command *bet* is used for this purpose. This is an example of how to use *bet*:

bet *anat_template.nii.gz output_bet_mask -m*

The result of this step is not precise enough and requires manual revision and correction of the obtained mask but once the binary mask and the anatomical template are available, the brain without skull is obtained using the command *fslmaths* as shown here:

fslmaths *anat_template.nii -mul output_bet_mask.nii anat_template_brain*

[14] https://github.com/ANTsX/ANTs/wiki/Forward-and-inverse-warps-for-warping-images,-pointsets-and-Jacobians

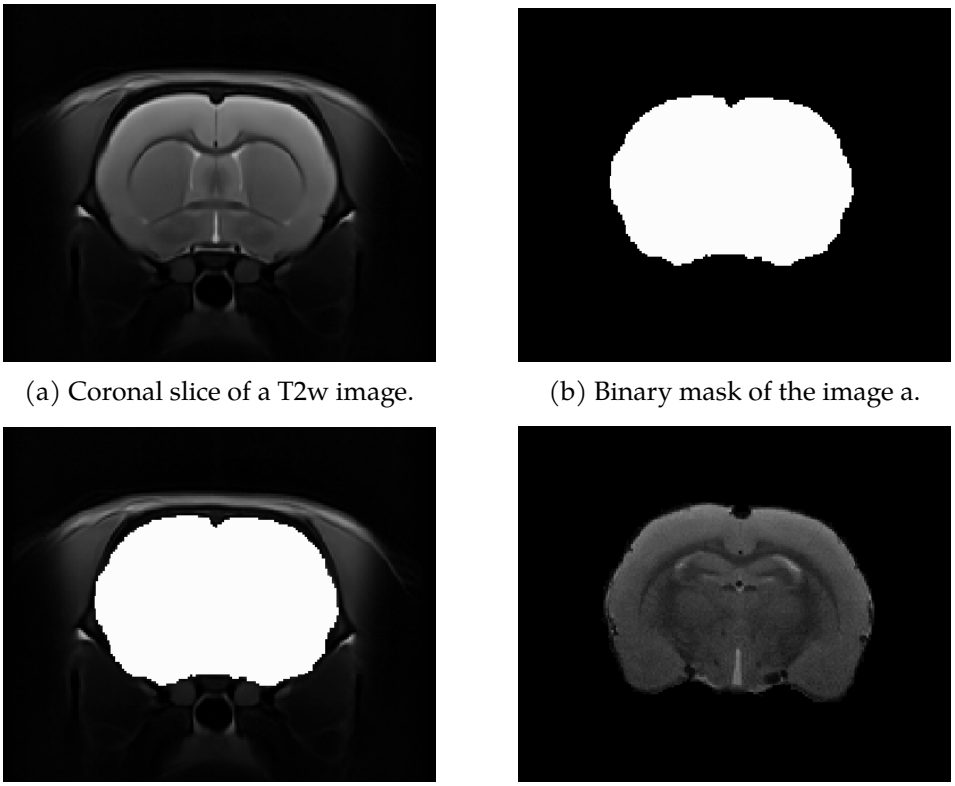

(a) Coronal slice of a T2w image. (b) Binary mask of the image a.

(c) Mask overlayed to the T2w image. (d) Resulting skullstripping (bet image).

Figure 11: **Skullstripping of an anatomical T2w image**. From a high-resolution anatomical T2w image, a binary mask (b) containing only the signal coming from the brain is obtained. From the multiplication of the binary mask with the T2w image (c) we obtain the image (d) bet, without skull.

Since we already have the brain extracted from the template and also the required transformations of each of the subjects with respect to the common template (result of step 5), it is possible to do the brain extraction of each of the subjects individually.

The function *antsApplyTransforms* is used on the mask of the template with the transformation file *Affine* and *InverseWarp* of each of the subjects. Once the mask has been transformed to the same space as the anatomical image (native space).

$$\textbf{\textit{antsApplyTransforms}} - d < dimensions > -i < input\_image > -o < output\_image > -t < transformations >$$

This example shows how to apply the mask transformations of the common space template on the anatomical image of a subject to its native space with the previously obtained files.

$$\textbf{\textit{antsApplyTransforms}}\ -d < 3 > -i < template\_mask > -r < native\_anat > -o < native\_anat\_mask > -t < native\_Affine > -t < native\_InverseWarp >$$

Summary of anatomical preprocessing

In this step it has been obtained: the anatomical template (common space) of the set of subjects, the binary mask of this one and this same template without skull, only with brain signal. With this also, each of the T2w images of each subject (native space) of the study without skull and with the bias field correction applied.

4.4.3 Functional preprocessing

Functional MRIs follow a set of corrections to improve the signal and the subsequent identification and interpretation of components at both, individual and group level.

Step 7. Functional skullstripping. The objective is to work only with the functional signal coming from the brain. For this purpose, the skullstripping of each of the volumes is performed. For that, an average volume is selected (in this case the images contain 600 volumes, so a volume around 300 is selected), used to extract the skull and also, as a reference in the Mcflirt method (Step 8. Head-motion correction at 4.4.3). This average volume is used to register the functional image to the anatomical one and thus work in the same space following the pipeline showed in figure 12. Once the registration is done and the transformation files are obtained, the transformation is applied to the rest of the volumes and the bet image is obtained in each of the native spaces.

Step 8. Head-motion estimation. Motion correction is performed using the Motion Correction using FMRIB's Linear Image Registration Tool (MCFLIRT) method of FSL. The tool loads the complete time series and uses the previously selected intermediate reference volume as the initial image for the template.
MCFLIRT performs successive searches and optimizations with different resolutions and tolerances to find the most accurate motion parameters. It also uses trilinear interpolation and an initial transformation assumption to improve the efficiency and quality of motion correction. In the initial low-resolution search, MCFLIRT assumes that there is no significant motion between the intermediate volume and the adjacent volume, and performs a fast search to obtain an initial estimate of the motion parameters.
The cost function in MCFLIRT is a measure used to evaluate the alignment of the images during the process of searching and optimizing the motion parameters. The cost function quantifies how well one image matches another in terms of similarity or discrepancy between the image data. The cost function used is the normalized correlation ('normcorr'). It is calculated using the normalized covariance of the pixel intensities. This measure takes into account the mean and standard deviation of the pixel intensities in both images, which allows a more robust comparison of the images. It is a popular choice in MCFLIRT due to its ability to handle intensity variations between images and its robustness in different motion correction scenarios.[29]

$$\textbf{\textit{mcflirt}} -in < inputImg > -out < output_mcf > - < refvol >< example_func > \\ -plots - mats - report;$$

Step 9. Spatial filtering To improve the signal to noise ratio, the FWHM (full width at half maximum) filtering method is applied. This spatial filtering method works as a convolution to smooth the signal. The kernel size is defined in terms of the width of the smoothing window. This value specifies the width of the Gaussian bell at half its maximum height. Several studies

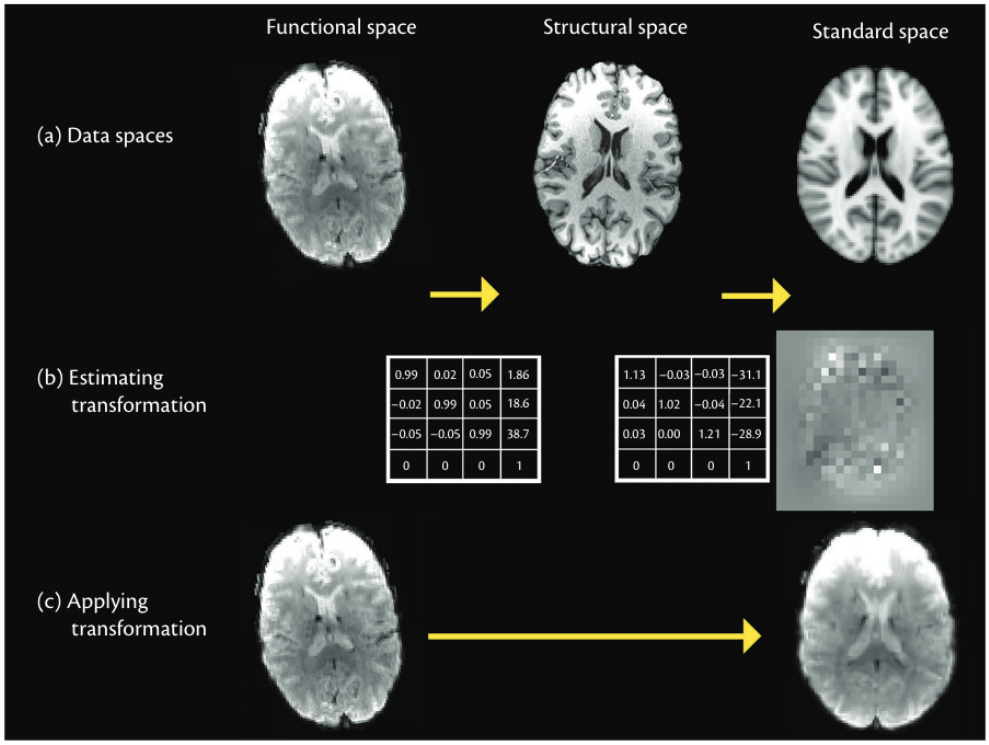

Figure 12: **Description of registration methods used to align data from different subjects into the same space.** (a) Images are obtained in distinct "spaces," highlighting a two-stage registration process. (b) In the initial stage of registration, the focus is on estimating the necessary transformations, which can take the form of linear matrices or non-linear warp images. (c) The second step of registration involves applying the transformation in order to resample an image into a different space. Through this process, The transformations can be combined and applied, thereby enabling the resampling of EPI functional data into a standardized space. Image obtained from [30]

differ on what is the correct size and value of kernel to use. Some recommend twice the pixel size while others are more conservative. The final choice is subjective and is based on the level of detail you want to maintain. A higher FWHM value results in stronger smoothing, while a lower value results in softer smoothing. For fmri studies where the specificity of connectivity is to be maintained, a kernel size not too large or close to the voxel size is chosen. A commonly used value for FWHM in rs-fMRI with a voxel size of 5x5x5 mm is about 6 mm which implies that the width of the Gaussian bell used will be about 6 mm at half its maximum height [31, 32]. There are also other studies such as Zilu et al.[33] where it is recommended to use twice the voxel size.
The way to apply this filtering has been by applying the AFNI blurfwhm method and trying different kernel sizes e.g. [6, 6, 6], [8, 8, 8], [10, 10, 10]. Each of the values refers to each dimension (x, y, z).

Step 10. Intensity normalization. Intensity normalization is performed to ensure that different fMRI images are comparable and on a consistent scale. Normalizing intensity involves scaling all fMRI images so that they have a common mean intensity and standard deviation. This is accomplished by adjusting the pixel intensities of each fMRI image to correspond to a reference scale.

The global intensity normalization is obtained by multiplying the signal by the scaling value. First the average intensity is calculated with the function **fsl.ImageStats()** and then it is scaled.

Step 11. High-pass filter Since there is no expected model of the signal, only drifts of frequencies lower than 0.01Hz are eliminated since the resting state signal oscillates between 0.01-0.1 Hz. When applying the filter, the cut-off frequency must be taken into account according to the TR:

$$\textit{Cutting\_freq} = 1(2 * TR)$$

Step 12. Melodic. Multivariate Exploratory Linear Optimized Decomposition into Independent Components (MELODIC) is an FSL tool that is used at both, single-subject and group level to decompose the fMRI signal into time-courses and spatial maps using Probabilistic ICA (PICA). It allows to classify and discard those noise components out of true neuronal signal.

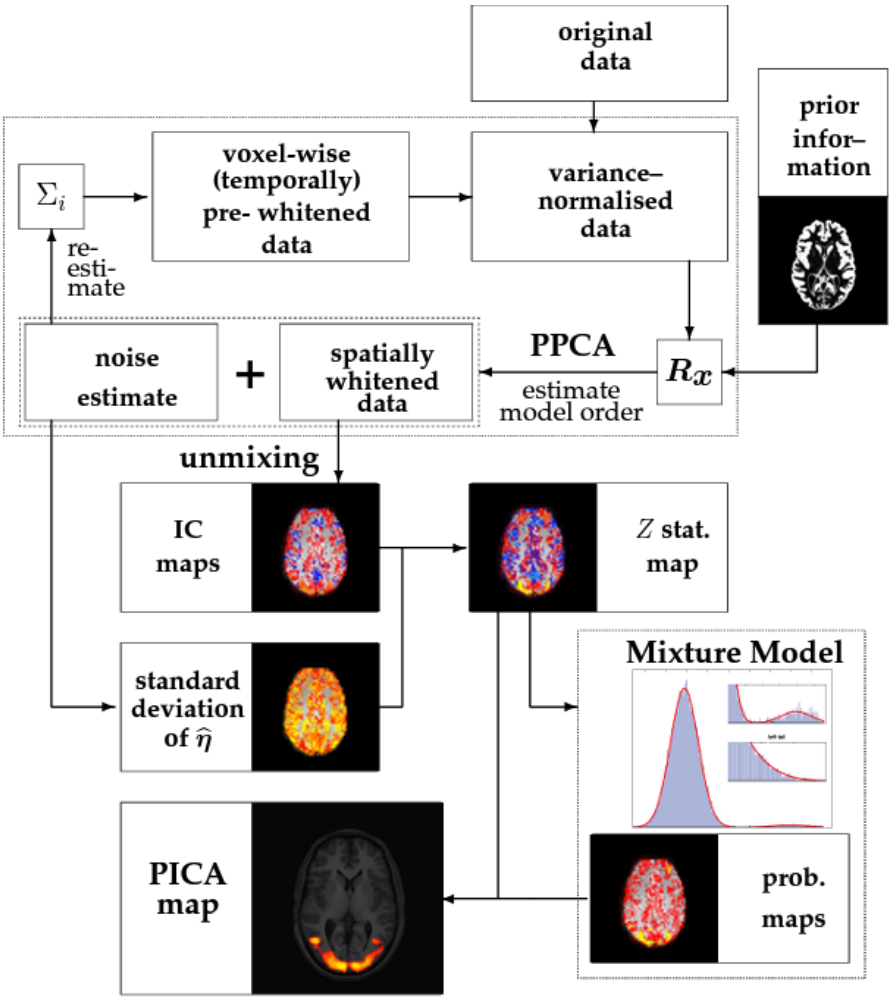

Figure 13: **Analysis steps involved in estimating the PICA model.** Image obtained from [34]

The classical ICA is a multivariate approach that analyses all voxels at once assuming that brain areas responsible for a particular task are independently distributed from brain areas responding to other sources of variability. In **classical ICA** there is no variable that accounts for noise so that can lead to overfitting compared to **Probabilistic ICA (PICA)**. PICA assumes that the

fMRI time series are generated from a set of fewer sources than observations in time statistically independent non-Gaussian sources (spatial maps) via a linear and instantaneous mixing process corrupted by additive Gaussian noise. First, the data is adjusted to have a uniform variance on a voxelwise basis and a covariance matrix is calculated. Probabilistic PCA (PPCA) is utilized to estimate the noise as well as a collection of orthogonal (uncorrelated) spatially whitened observations. This method also allows for the determination of the ICs' dimensionality, although it can sometimes be set by the user. The noise covariance structure can be estimated from the residuals to temporally pre-whiten and re-standardize the data [35]. By applying PPCA to the spatially whitened observations, individual component maps are generated using a modified fixed-point iteration technique called FastICA[36]. This optimization process aims to maximize negative entropy in order to identify non-Gaussian sources. Subsequently, these maps are transformed into Z-scores, which are influenced by the amount of variability explained by the entire decomposition at each voxel, relative to the residual noise. In other words, they represent the extent to which the signal explained within this model fits the data. Lastly, Gaussian or Gamma mixture models are fitted to the individual Z-maps to determine spatial locations that exhibit significant modulation by the associated timecourse (figure 13).

The purpose is to run a single-subject analysis to clean data by removing components related to noise(e.g. motion, physiological noise).The tool receives as input a preprocessed 4D rs-fMRI image and the number of components. In this case, taking as reference the resting state networks shown in figure 8, it has been specified 15, 20 and 25 components. It is also important to take into account the number of components of the ICA. With larger dimensions, the signal may be segmented into several components, while with a very low number of dimensions, noise and signal may be mixed in the same component.

Step 13. Noise classification and removal The labeling and classification of the components is done manually. As explained in Griffanti et al.[37], special attention should be paid for each component to **1. the spatial maps**, **2. the time course** and **3. the power spectrum** of the time course to identify which components are signal and which are noise. An example of the classification of noise components is shown in figure 14 and in figure 15, signal.

After classification, the noise components are removed by using the **fsl_regfilt** command. It is a tool that allows the elimination of confounding variables or artifacts from functional time series data using a design matrix and linear regression.

$$\textbf{\textit{fsl\_regfilt}} -i < filtered\_data > -d < melodic\_mix > -o < output\_clean > -f < 1, 2, 3 >$$

The command expects the preprocessed functional image (*-i*), the file containing the matrix of temporal mixtures of the identified principal components (*melodic_mix*) and the components classified as noise (*-f*).

The last step is to register all the fMRI images to a common space, in this case, to the anatomical template created from all the study subjects, and then proceed to the analysis.

Summary of functional preprocessing

To summarize, the most important steps followed in the preprocessing of fmri images have been: spatial filtering, temporal filtering, intensity normalization and removal of artifacts (e.g. motion) by component extraction. Now the fmri images are preprocessed, in a common space and ready to perform any kind of analysis.

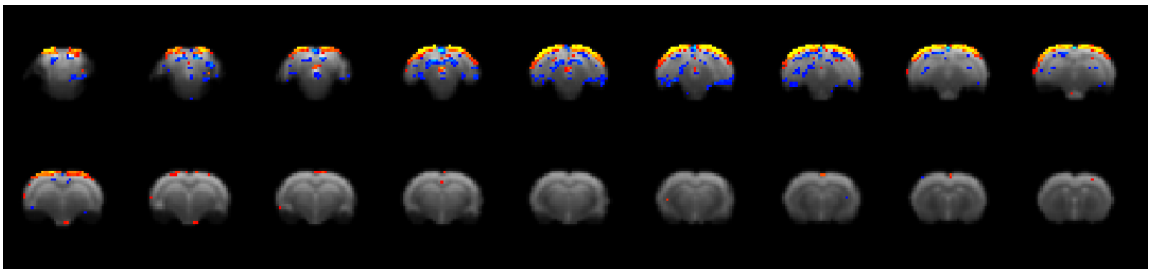

(a) Coronal view of an spatial map of a noise component overlapping into a T2w image.

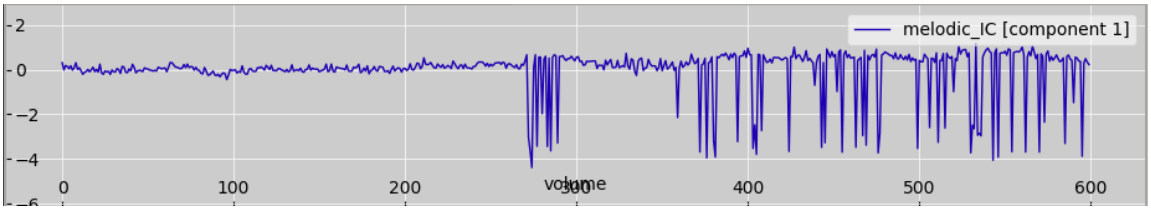

(b) Time course of a noise component. X-axis, fMRI volumes (one per TR) and Y-axis, the demeaned signal intensity.

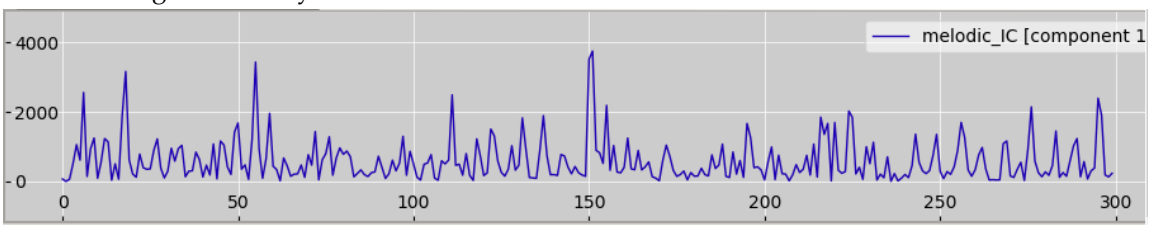

(c) Power spectrum representation of the noise component.

Figure 14: **Example of a noise component of a single-subject ICA.**

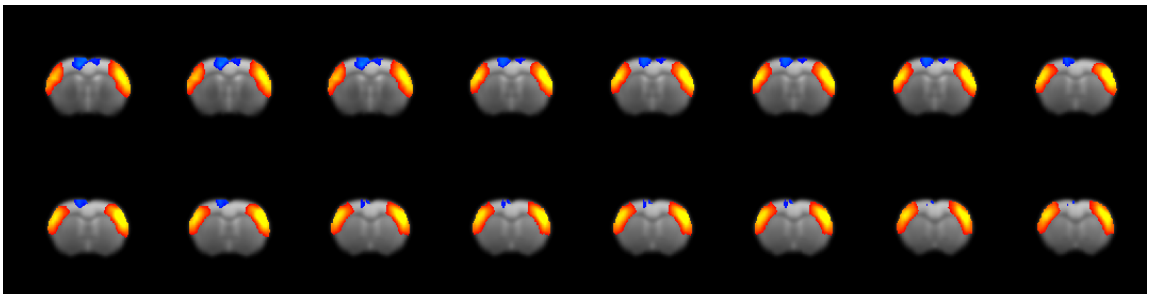

(a) Coronal view of an spatial map of a signal component overlapping into a T2w image.

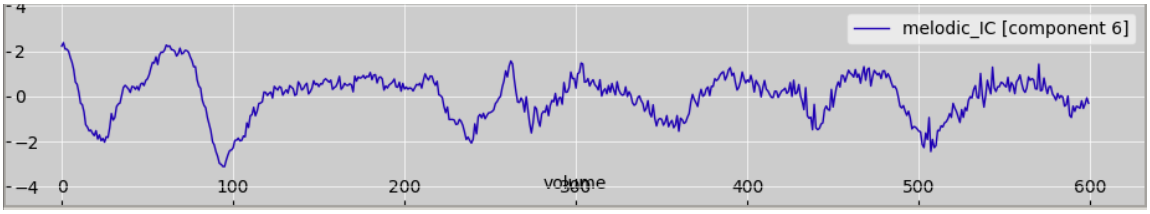

(b) Time course of a signal component. X-axis, fMRI volumes (one per TR) and Y-axis, the demeaned signal intensity.

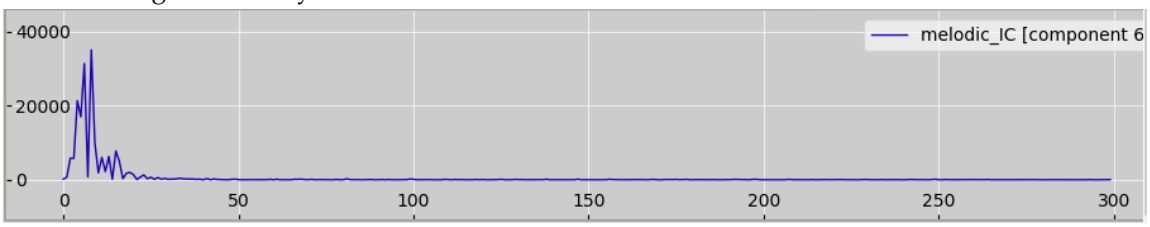

(c) Power spectrum representation of a signal component.

Figure 15: **Example of a signal component of a single-subject ICA.**

4.5 Independent Component Analysis

While the seed-based method provides a single connectivity measure for each pair of regions, the ICA method provides three connectivity measures: total connectivity, connectivity within networks, and connectivity between networks. As the target is to study and detect whole-brain RSNs, we choose to use ICA [38].

4.5.1 Group ICA

To obtain the group RSNs a group ICA is performed (see code 2 adapted from the tool RABIES) using the **melodic** tool of FSL (previously explained in step 12, chapter 4.4.3). After preprocessing the images in a subjet-level and registering all of them to a common space they are merged in the fourth dimension (e.g. using ***fslmerge*** *-t output* [*list_files*] where '-t' means merge volumes in time).

The melodic command expects as input the ICA decomposition dimensionality, the 4D concatenated volumes, the TR in seconds and the output directory. It returns a 4D image, *melodic_IC.nii*, where each volume corresponds to an independent component.

Different dimensions are tested to extract components, from 20 to 75. The higher the dimensionality, the more segregated the results, whereas, if the dimensions are very low, networks may overlap.

Listing 2: Code in Python to run group ICA.

```
def run_group_ICA(bold_file_list, mask_file, dim, random_seed):
    file_path = os.path.abspath('filelist.txt')
    merged = flatten_list(list(bold_file_list))
    df = pd.DataFrame(data=merged)
    df.to_csv(file_path, header=False, sep=',', index=False)

    out_dir = os.path.abspath('group_melodic.ica')
    command = f'melodic -i {file\_path} -m {mask_file} -o {out_dir} -d {dim} --report --seed={str(↩
        ↪ random_seed)}'
    rc = run_command(command)
    IC_file = out_dir+'/melodic_IC.nii.gz'
    return out_dir, IC_file
```

4.5.2 Dual regression

Dual regression is used to investigate functional connectivity networks in the brain from an individual point of view to examine group differences. It is divided into two main stages (figure 16: the first stage is the spatial decomposition and the second stage is the temporal decomposition.

Stage 1. Subject-specific time courses are calculated from the groupICA spatial maps. Here, the IC maps obtained in the previous stage are used as templates or regressors to determine the contribution of each component to each voxel over time. A linear regression is performed on each voxel to estimate the time series corresponding to each IC. The output is a *.txt* file per subject, each containing columns of time series, one per group-ICA component.[39]

Stage 2. Using the subject-specific time courses output of the step 1, the subject-specific spatial maps are calculated conducting a multivariate temporal regression.
At this stage, the spatial beta maps as a 4D image file per subject (*dr_stage2_subject*[*#SUB*].*nii.gz*) and the Z-stat version (*dr_stage2_subject*[*#SUB*]*_Z.nii.gz*) are obtained. This beta spatial maps represents the strength and direction of the relationship between the independent variable and

brain activity in each voxel, while Z maps indicate the statistical significance of these effects in terms of the standard deviation of the population mean.[39]

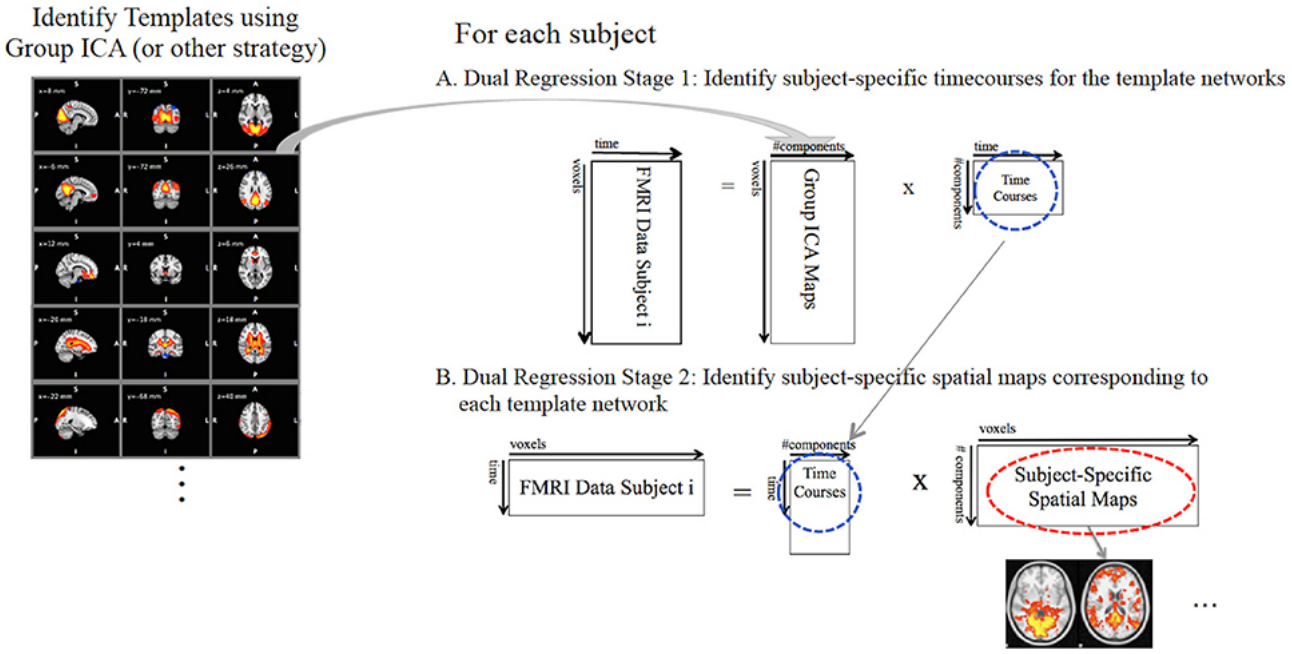

Figure 16: **General dual regression workflow.** Figure obtained from [39]

4.5.3 Statistical analysis

With the FSL tool it is possible to perform various statistical analyses using Generalized Linear Model (GLM). GLM[15] is used to model the relationship between a set of independent variables (predictors) and a dependent variable. In fMRI it is used to investigate relationships between imaging signals and variables of interest, such as experimental conditions, clinical covariates or measures of brain connectivity. Statistical analyses grouping data by sex or age condition are included in a second-level type of analysis. The GLM adjusts the data to assess common differences or effects at the group level.

Using the subject-specific spatial beta maps estimated in stage 2 of the dual regression, a between-subjects analysis is performed to calculate the differences in FC between the different independent components by analyzing the correlation or covariance between their time series.

Depending on the question to be studied, a group-level design has to be designed to make comparisons. In this case, we want to determine whether:

1. There are group differences according to sex. In this analysis all the subjects of the study, n=38, are added, of which there are 21 females and 17 males. This corresponds to a two-group unpaired analysis where the two sex groups are contrasted and the age of the subject is added as a covariate. The configuration of the model according to the Glm tool is the one showed in figure 17a.

[15]GLM https://fsl.fmrib.ox.ac.uk/fsl/fslwiki/GLM

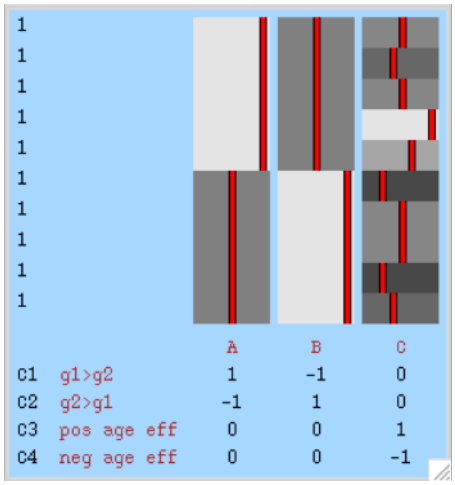

(a) Two-Group Difference Adjusted for Covariate

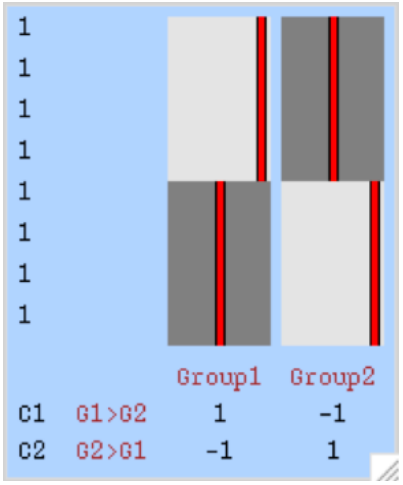

(b) Two-Group Difference

Figure 17: **Representation of the model configuration through the graphic interface of Glm.** a) Two-Group Difference Adjusted for Covariate model. The two-group contrast (G1 and G2) is defined and a third contrast with a covariate is added. b) Two-Group Difference. Contrast of two-group (G1 and G2).

2. There were differences between two age groups regardless of sex. In this analysis, the effect of age is contrasted between two points. First, the effect on the two extreme times (P210 vs. P546) and then, the evolution studying the intermediate steps (P210 vs. P364 and P364 vs. P546). This analysis is a two-group difference analysis (figure 17b).

2nd Analysis			
	P210	P364	P546
P364	29	-	25
P546	22	29	-

Table 1: Data distribution for 2nd statistical analysis.

4.5.4 FSLNets - Inter-network connectivity

From the time series obtained in stage 1 of the dual regression it is possible to perform basic network modeling with the FSL extension, FSLNets[16]. It allows the calculation of connectivity measures, such as the functional correlation matrix and network connectivity matrices, as well as the performance of modularity and connection density analyses. It is possible to explore the organization of networks and how different brain regions interact with each other.

The tool needs the individual time series of each subject, the TR and the groupICA output file, *melodic_IC.nii* (line 2 of code 3). In this way all the time series of all subjects and the time spectra of the RSNs are loaded.

To obtain the network matrix, or netmap, for each subject, the correlations between pairs of time series are calculated (lines 8-9 of code 3). In addition, the group average network matrix is also

[16]https://fsl.fmrib.ox.ac.uk/fsl/fslwiki/FSLNets

extracted (lines 12-13 of code 3). This command stores the simple average of netmats across all subjects (Mnet) and the results of a simple one-group t-test (against zero) across subjects as Z-values (Znet).

The nodes, RSNs, are grouped in a hierarchy based on their covariance structure to form larger resting state networks (line 16 of code 3).

To finish, a comparison is made between groups as to whether the netmaps differ significantly with a two-sample t-test (line 19 code 3). This is a 'univariate' test, as you test each edge of the network matrix separately for a group-difference, and then estimate p-values for these tests, correcting for multiple comparisons across all edges. The design files (design.con/mat) are the same as those used in the previous analyses (section 4.5.3) where we compared two age groups.

Listing 3: FSLNets Matlab code.

```
# Networks estimation
ts = nets_load('groupICA25.dr', 2, 2); # load timeseries from DR output

ts_spectra = nets_spectra(ts); # temporal spectra of RSNs
ts = nets_tsclean(ts,1); # cleaning components

# Calculating netmats for each subject
Fnetmats = nets_netmats(ts,1,'corr');
Pnetmats = nets_netmats(ts,1,'ridgep',0.1);

# Group-average netmat summaries
[Znet_F,Mnet_F]=nets_groupmean(Fnetmats,0);
[Znet_P,Mnet_P]=nets_groupmean(Pnetmats,1);

# Group average network hierarchy
nets_hierarchy(Znet_F,Znet_P,ts.DD,'groupICA100.sum');

# Cross-subject comparison with netmats
[p_uncorr,p_corr]=nets_glm(Pnetmats,'design/unpaired_ttest_1con.mat','design/unpaired_ttest_1con.con',1);
nets_edgepics(ts,'groupICA25.sum',Znet_P,reshape(p_corr,ts.Nnodes,ts.Nnodes),1);
```

5 Results

5.1 Resting State Networks

As mentioned in section 4.5.1, by applying the group-level ICA analysis, the following RSNs have been identified as reported in figure 8, as identified in Grandjean, J. et al.[27]: hippocampal, motor, somatosensory (mouth), somatosensory(bf), visual, parietal associative, restrosplenial, auditory, cingulate/prelimbic and cerebellum (figure 18).

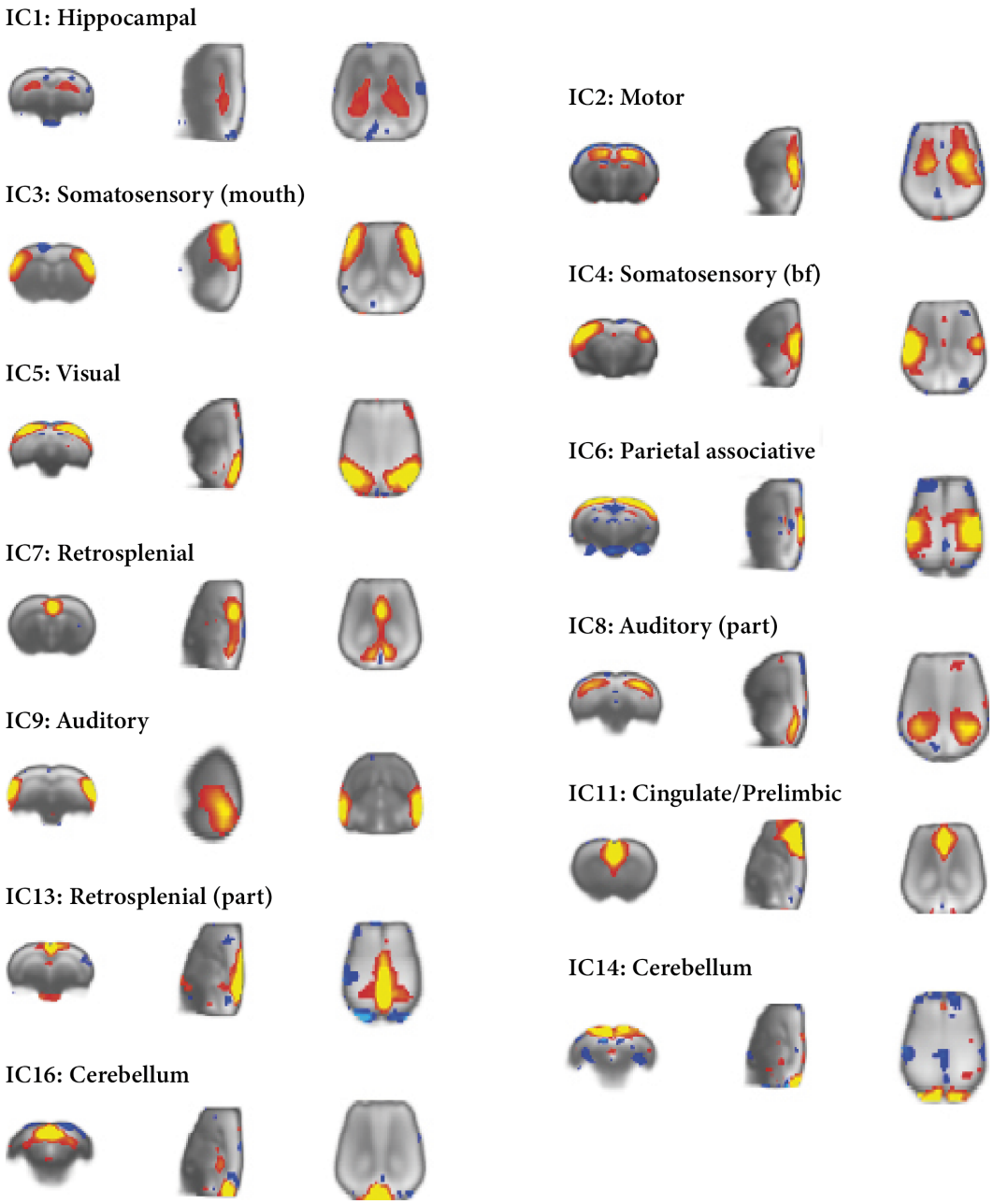

Figure 18: **Identified RSN by group ICA analysis.**

5.2 Group level differences

According to the subject-level statistical analysis versus the group RSN, the results for the different analyses are as follows:

1. **Group differences according to sex.**

   The first statistical analysis (Two-Group Difference Adjusted for Covariate model) compared, for each of the RSNs (components of the ICA) and all subjects, the betas across sexes and treating age as a covariate. This analysis indicated that there were no significant sex differences in the contribution to the group networks. Therefore, the following analyses focused on assessing the contribution and changes as a function of age by pooling together animals of both sexes. Without taking sex into account in the analysis, we avoided losing statistical power to detect significant effects.

2. **Group differences grouped by age.**

   In this analysis, Two-Group Difference model, the effect of age was compared for each of the RSNs in 3 conditions: **(I) P210 vs P546**, **(II) P210 vs P364** and **(III) P364 vs P546**.

   The first analysis, which compares the time points P210 vs P546, is intended to study whether or not there are changes in the FC of the RSNs between the two more extreme conditions. Many of them show significant differences according to age, resulting in a higher FC of the networks at age 546. Afterwards, we compared the changes of this FC between the extreme points and the intermediate one to characterize the temporal evolution. Table 2 shows a summary of the results.

Age (days)	IC1	IC2	IC3	IC4	IC5	IC6	IC7	IC8	IC9	IC11	IC13	IC14	IC16
(I) 210 vs 546	NS	↑	NS	↑	↑	NS	NS	↑	↑	↑	NS	NS	NS
(II) 210 vs 364	NS	NS	↓	↓	NS	↓	↓	NS	↓	NS	↓	NS	NS
(III) 364 vs 546	NS	↑	↑	↑	↑	↑	↑	↑	↑	↑	NS	NS	NS

Table 2: **Statistical FC analysis results.** NS: Non statistically significant, ↑ : statistically significant increase in FC with age and ↓ : statistically significant decrease in FC with age.

In general, the FC decays significantly in certain areas between 210 and 346 days. These reductions afterwards, from 364 to 546, undergo the opposite effect and the FC increases significantly.

Figures 19 to 22 show the maps with the most significant areas of change for the different networks and analyses. To represent and interpret the output statistical contrast maps we display the values comprised between 0.95 and 1 (corresponding to 1 - p value).

5.3 Inter-network connectivity

As described in section 4.5.4, by analyzing the frequency spectrum, it is possible to differentiate between CIs related to noise and those related to RSNs. For a proper interpretation of an RSN, the frequency spectra should fall off smoothly as the frequency increases as shown in figure 23.

By analyzing FC between networks taking into account the correlation between them, the effect of age on connectivity is tested. In this way, networks are grouped according to their covariance

and how functionally connected they are. In figure 24 it can be seen how the groups of networks are maintained over the time, identifying four main groups:

1. Motor(2), Somatosensorial(mouth)(3), Somatosensorial(bf)(4) and Parietal associative(6).
2. Visual (5) and Auditive (8 - 9)
3. Cingulate (10) and Retrosplenial (7 - 11)
4. Hipoccampal (1) and Cerebellum (12 - 13)

These clusters depict the strong positive connectivity forming larger networks. Dark red squares indicate strong positive correlations, light green indicates a correlation close to 0 and dark blue represents a strong negative correlation. Full correlations between pairs of networks are shown below the diagonal line (in gray), while partial correlations are shown above the diagonal line.

(a) Motor RSN (364 vs 546)

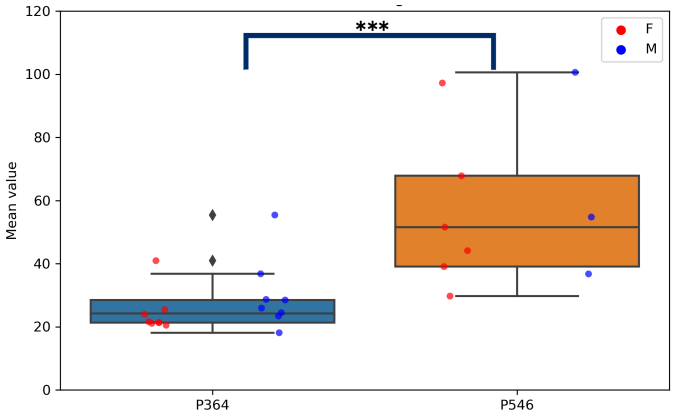

(b) Mean FC difference between 364 and 546 days in motor RSN.

(c) Visual RSN (364 vs 546)

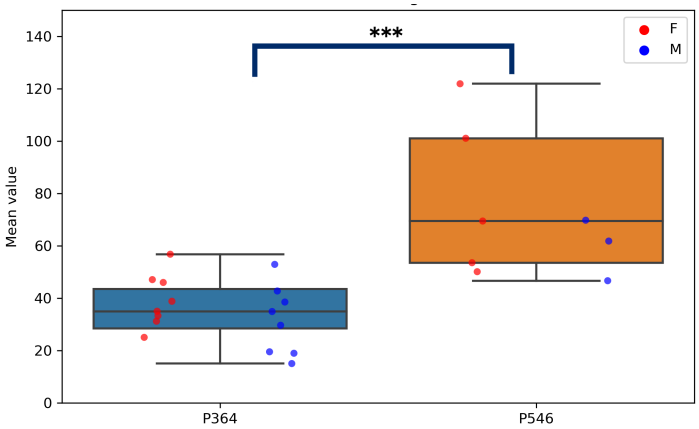

(d) Mean FC difference between 364 and 546 days in visual RSN.

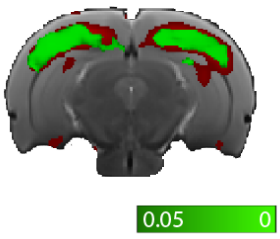

(e) Auditory RSN (364 vs 546)

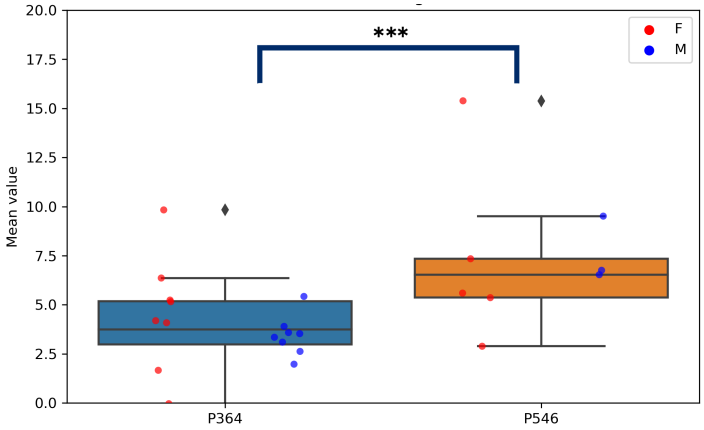

(f) Mean FC difference between 364 and 546 days in auditory RSN.

Figure 19: **Statistically significant difference in FC between two age points in a) Motor, c) Visual and d) Auditory RSNs.** Representation of mean fc values per subject in the areas of significant change contrasting 364 and 546 days (subfigures b, d and f). Blue dots represents males and red female subjects. Box and whiskers represents the 25-75% of the values and the scores outside the middle 50% respectively. T-test, * $p<0.05$, ** $p<0.01$ and *** $p<0.001$.

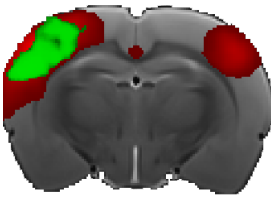

(a) Somatosensory (bf) RSN (210 vs 364)

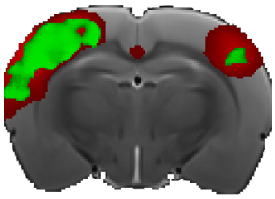

(b) Somatosensory (bf) RSN (364 vs 546)

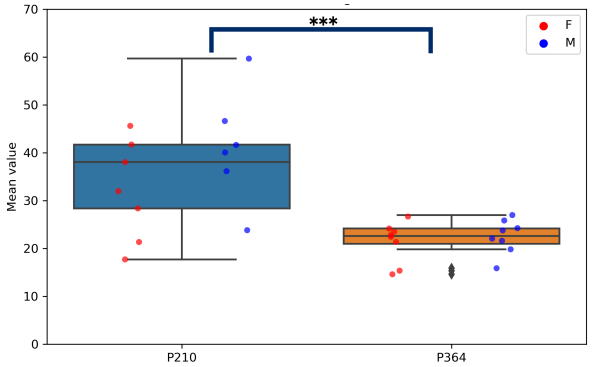

(c) Mean FC difference between 210 and 364 days in somatosensory (bf) RSN

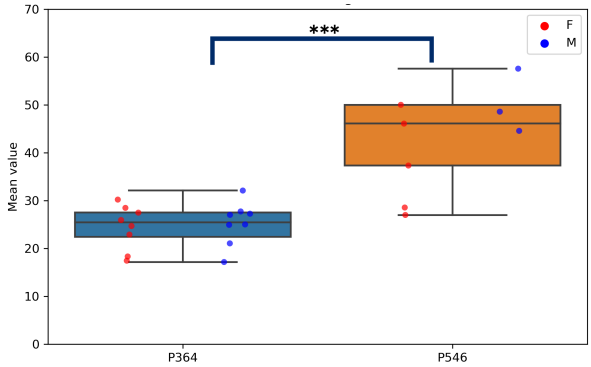

(d) Mean FC difference between 364 and 546 days in somatosensory (bf) RSN

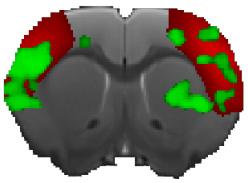

(e) Somatosensory (mouth) RSN (210 vs 364)

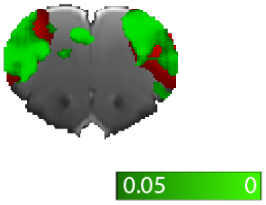

(f) Somatosensory (mouth) RSN (364 vs 546)

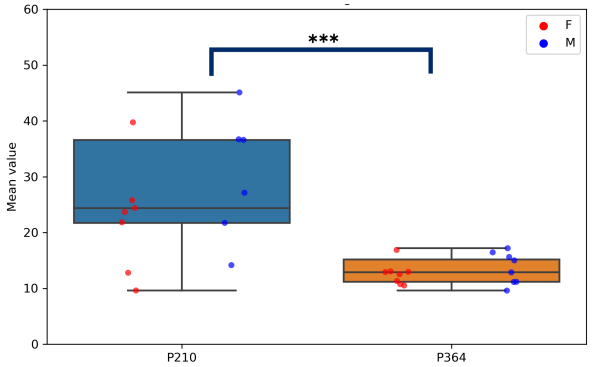

(g) Mean FC difference between 210 and 364 days in somatosensory (mouth) RSN.

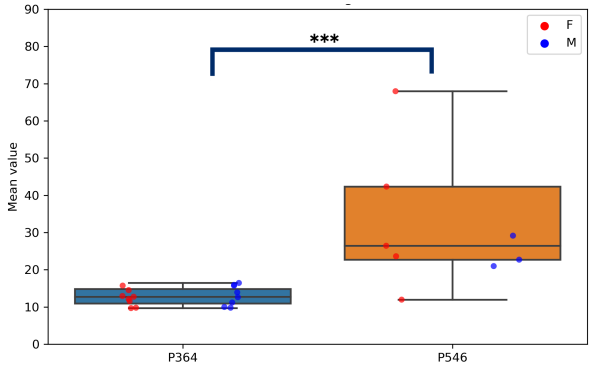

(h) Mean FC difference between 364 and 546 days in somatosensory (mouth) RSN.

Figure 20: **Statistically significant difference in FC between two age points in a) and b) Somatosensory (bf) and e) and f) Somatosensory (mouth) RSNs.** In green, a) and e) and b) and f) represents the areas of significant change in FC contrasting 210-364 and 364-546 days respectively. Representation of mean FC values per subject in the areas of significant change contrasting, c) and g) 210 and 364, and in d) and h) 364 and 546 days. Blue dots represents males and red female subjects. Box and whiskers represents the 25-75% of the values and the scores outside the middle 50% respectively. T-test, * $p<0.05$, ** $p<0.01$ and *** $p<0.001$.

(a) Parietal associative RSN (210 vs 364)

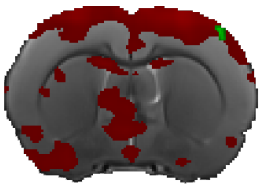

(b) Parietal associative RSN (364 vs 546)

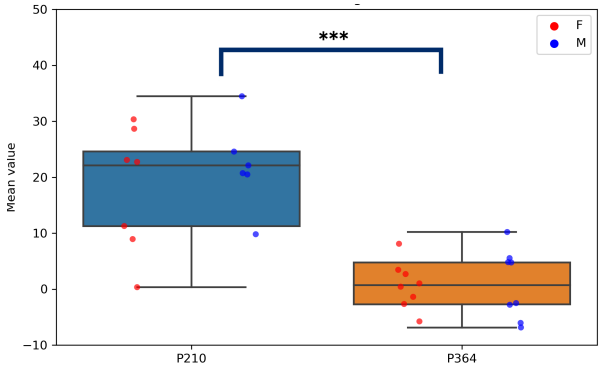

(c) Mean FC difference between 210 and 364 days in parietal associative RSN

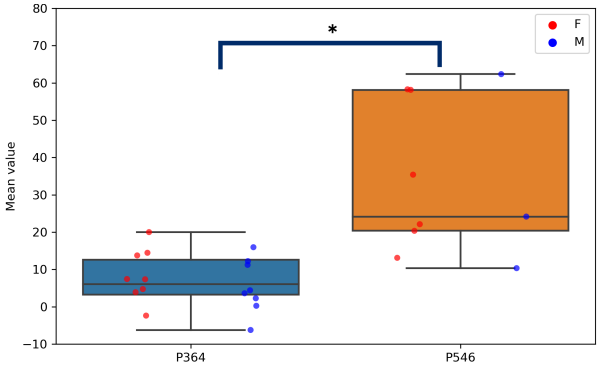

(d) Mean FC difference between 364 and 546 days in parietal associative RSN

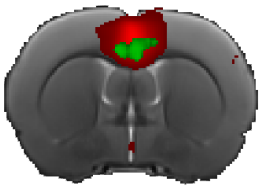

(e) Retrosplenial RSN (210 vs 364)

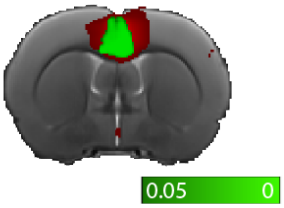

(f) Retrosplenial RSN (364 vs 546)

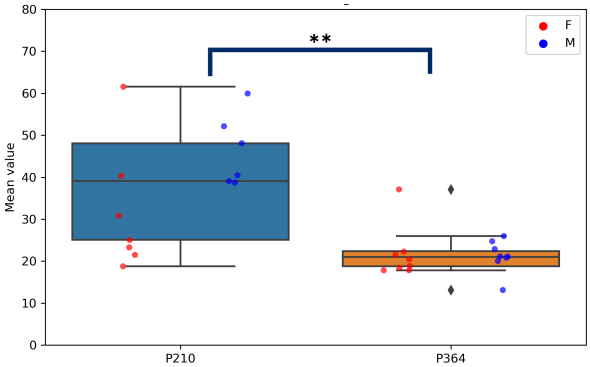

(g) Mean FC difference between 210 and 364 days in retrosplenial RSN

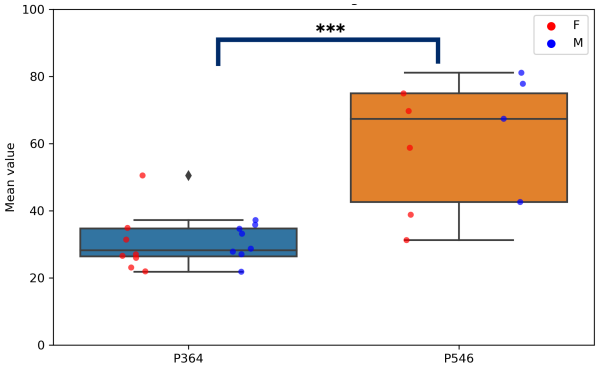

(h) Mean FC difference between 364 and 546 days in retrosplenial RSN

Figure 21: **Statistically significant difference in FC between two age points in a) and b) Parietal associative and e) and f) Retrosplenial RSNs.** In green, a) and e) represents the areas of significant change in fc contrasting 210-364 and b) and f) 364-546 days respectively. Representation of mean fc values per subject in the areas of significant change contrasting, c) and g) 210 and 364, and in d) and h) 364 and 546 days. Blue dots represents males and red female subjects. Box and whiskers represents the 25-75% of the values and the scores outside the middle 50% respectively. T-test, * $p<0.05$, ** $p<0.01$ and *** $p<0.001$.

(a) Auditory RSN (210 vs 364)

(b) Auditory RSN (364 vs 546)

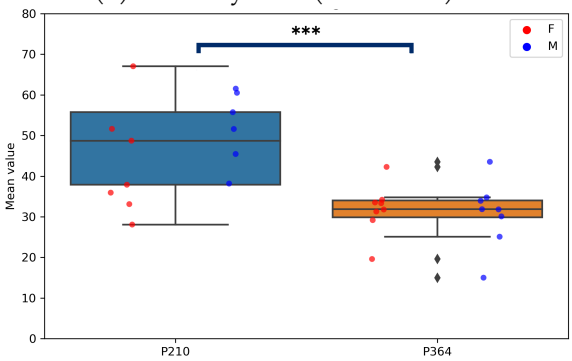

(c) Mean FC difference between 210 and 364 days in auditory RSN

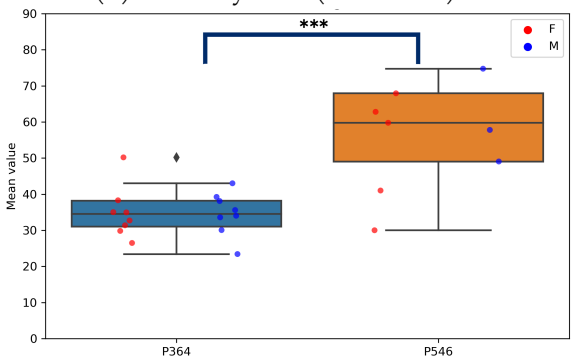

(d) Mean FC difference between 364 and 546 days in auditory RSN

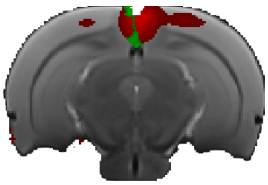

(e) Retrosplenial (part) RSN (210 vs 546)

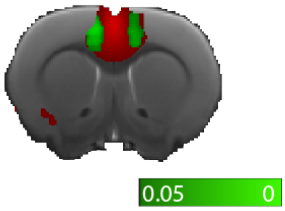

(f) Cingulate/Prelimbic RSN (364 vs 546)

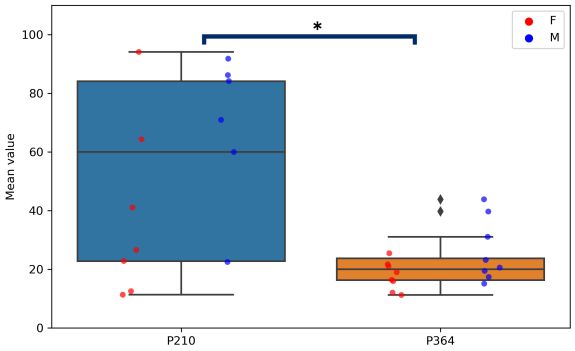

(g) Mean FC difference between 210 and 364 days in retrosplenial RSN

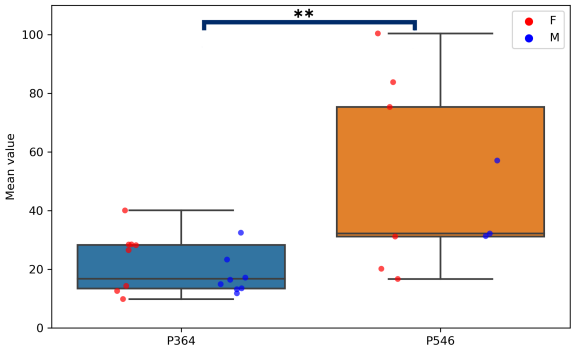

(h) Mean FC difference between 364 and 546 days in cingulate/prelimbic RSN

Figure 22: **Statistically significant difference in FC between two age points in a) and b) Auditory and e) and f) Cingulate/Prelimbic RSN.** In green, a) and e) represents the areas of significant change in fc contrasting 210-364 and b) and f) 364-546 days respectively. Representation of mean FC values per subject in the areas of significant change contrasting, c) and g) 210 and 364, and in d) and h) 364 and 546 days. Blue dots represents males and red female subjects. Box and whiskers represents the 25-75% of the values and the scores outside the middle 50% respectively. T-test, * $p<0.05$, ** $p<0.01$ and *** $p<0.001$.

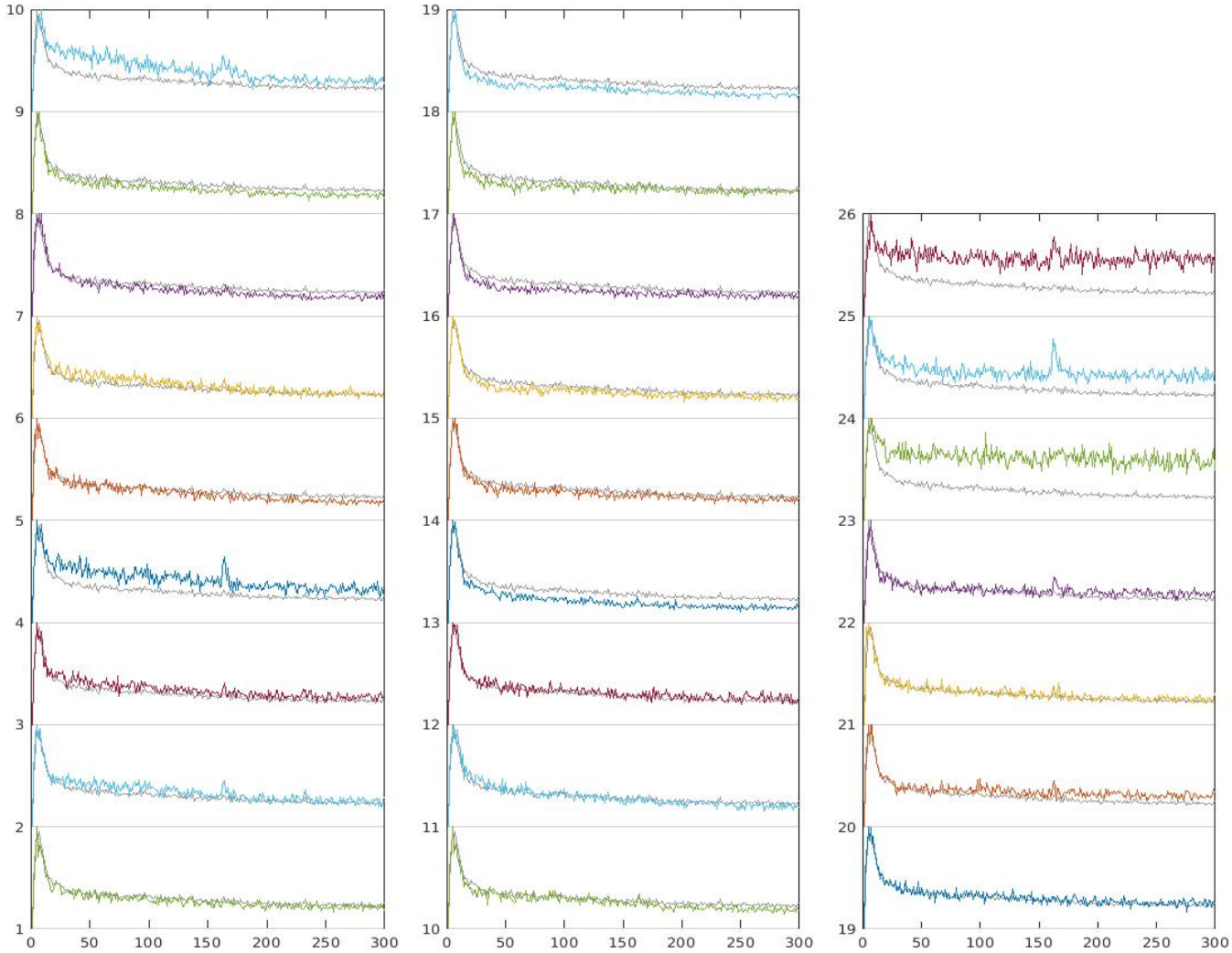

Figure 23: **Nodes frequency spectra.** Colored, group averaged frequency spectra of individual nodes (group independent components). In light gray line, average across all nodes.

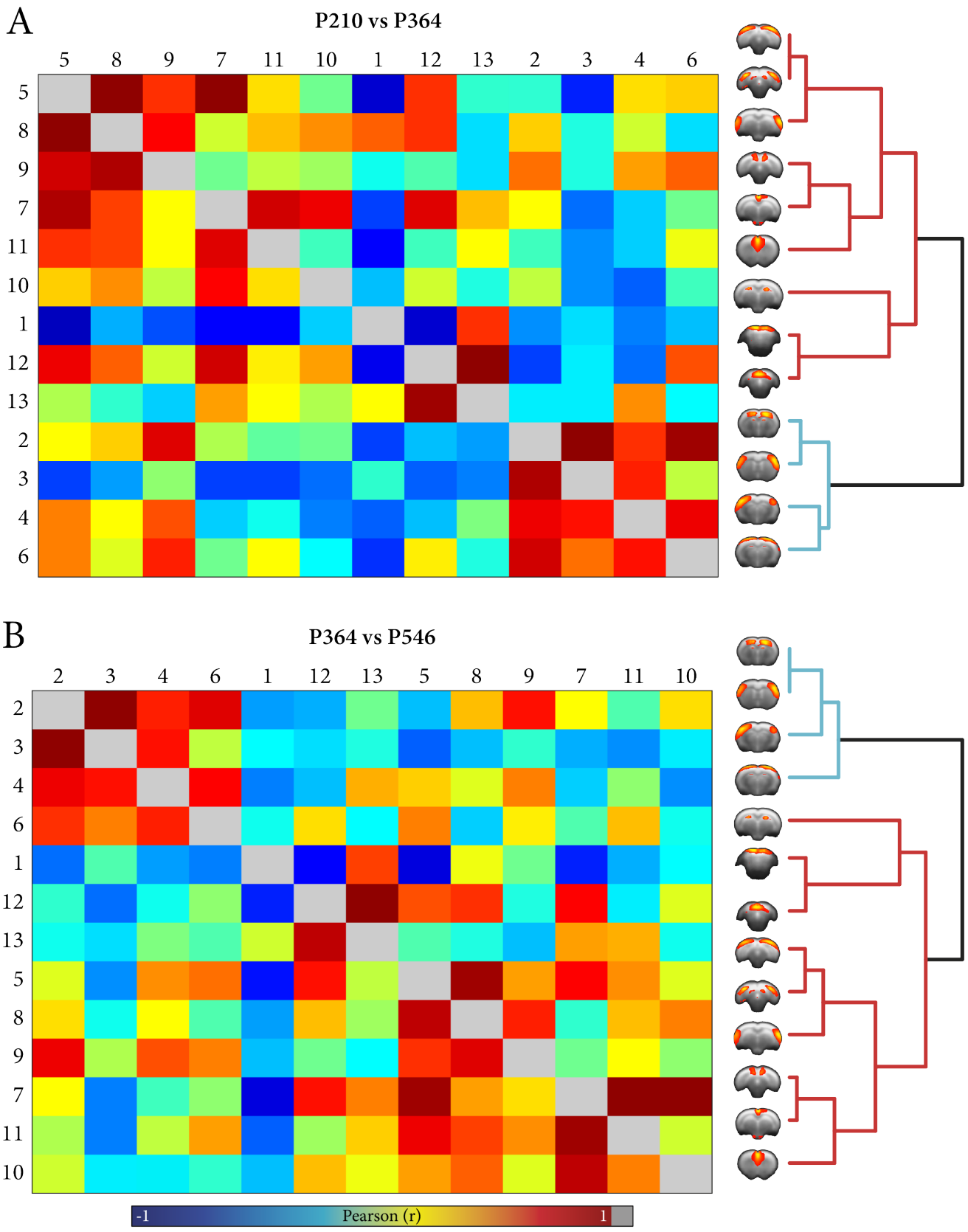

Figure 24: **Group average network hierarchy.** Clustering tree of RSN group nodes based on covariance for A) P210-364 and B) P364-546 groups. Full correlations are shown below the diagonal line with partial correlations shown above the diagonal line.

ETSEIB

6 Discussion

With aging our brain undergoes structural and functional changes which, late in life, translate into cognitive deficits such as reduction of processing speed, long-term memory and other alterations, as discussed in the section 2.2. MRI in rodents is a unique tool to characterize brain changes longitudinally, due to its non-invasiveness, versatility and to the limited lifespan of rodents. As such, we report here preliminary results of an fMRI experiment aiming at characterizing functional connectivity at different ages and for animals of both sexes.

A large number of longitudinal aging studies, both in animal models and humans, focus on the study of functional connectivity using seed-based analysis [40, 41, 42]. The use of these analyses allows studying functional connectivity with respect to specific brain areas selected a priori. In contrast, in our analysis, we identify patterns of brain activity in a data-driven fashion. Unlike seed-based analysis, ICA automatically identifies components that explain the majority of variability in fMRI data. This has the advantage of identifying intrinsic functional brain networks, including those that may not have been previously known or considered relevant. Additionally, the bold signal during evoked activity [43] or task-dependent activity [44] is expected to have a more temporally defined and localized form compared to the bold signal during resting state, where the brain exhibits spontaneous but organized activity patterns. Since the objective is to understand the patterns of functional connectivity in aging with a global perspective, we chose an unbiased approach.

The first result of the study is that our framework is capable of capturing the evolution of functional connectivity from adulthood to early senescence. In fact, our data include animals from 210 days, the stage at which brain maturation is completed and the rats are considered adult (the equivalent of about 18 years old in humans) to 546 days, when rats are already undergoing senescence (corresponding to about 45-50 years old for humans [45]). Despite some inevitable differences, rats and humans share several key aspects of their functional connectivity during resting state. In fact, several networks are present in both species (e.g. the default mode network mentioned in section 2.1.3), attend to similar functions and present comparable behaviour in terms of inter-networks connectivity. All this justify the use of rodents as a good model to investigate changes in functional connectivity between networks happening with age.

Our data show that the hierarchy between networks, measured as similarity in their connectivity, remains mostly unaltered over time (figure 24). Visual and auditory networks on one side, and motor and somatosensory networks on the other, are strongly related as can be seen in (figure 24). The functional communication between these regions is important for performing cognitive processes by integrating information from different regions[46]. Another important connectivity hub that emerged from our data is the retrosplenial and visual networks (5 and 7 columns in figure 24). Several studies such as Ash, J. A. et al. [47] in the rodent model showed a positive FC maintained in retrosplenial network. In contrast, (figures 21f and 21h) show that the FC increases significantly with age. This network is responsible for the integration of sensory, motor and visual information and is related to the changes obtained in other networks[48].

Certain areas of the brain increase their functional connectivity significantly as a compensatory mechanism for aging-reared microstructural alterations. As mentioned in previous researchs, due to the deterioration of brain microstructure, a higher activation can become necessary to maintain certain functions[49, 15]. According to our data, the somatosensory, retrosplenial and auditory RSNs reduce their functional connectivity in different areas between 210 and 364, but

increase their functional connectivity between 364 and 546 (figures 20, 21 and 22). Visual and sensory functions in humans get worse with age, causing mobility impairments. These changes can be underlying the increase in connectivity of the motor network (figure 19a). This effect in humans has been explained with the The Scaffolding Theory of Aging and Cognition compensation theory. This theory focuses on a generalized increase in frontal activation with age as a marker of an adaptive brain involved in compensatory scaffolding in response to challenges posed by declining neural structures and function [15]. The same pattern of compensation is also evident in the auditory network [50], as seen in the figure 19e.

In our data, the FC increases significantly in the motor network. With ageing, there is a well known impaired motor ability. Human literature reported both increase [51] and decrease [52] in the motor FC network. In line with the hypothesis of adaptative remodeling, task-fMRI experiments have shown evidence that older subjects recruit a wider network of brain regions during the performance of various motor tasks in an attempt to maintain parity of performance levels with their younger counterparts [51].

Analyzing the sex effect in the differences in functional connectivity does not show significant impact of sex in any of the localized RSNs. Indeed, the literature reports sex differences where, for example, female middle-age rats, outperform males on a temporal episodic memory task[53]. However, when looking at FC changes, Febo, Marcelo, et al.[54] and others [55, 56] found no sex-dependent changes. One of the possible causes for the lack of significant sex effects may be relatively low sample size; further studies are needed to clarify this point.

Another important factor to take into account is individual variability. Some animals show more pronounced changes compared to others in the same network and age group (see figure 22h). The mean values of change are quite different between subjects. It would be interesting to relate this inter-individual variability to individual performance in behavioural tasks, and also to other characteristics like grey and white matter integrity. Similar interindividual variability is also observed in humans, where a portion of the individuals have preserved memory and function even at late stages of life.

An important factor is the dimensionality of the group ICA because its correct choice is crucial to identify and interpret the RSNs found (figure 18). Selecting a dimension too big would result in fragmenting a RSN into several unidentified components; on the other hand, selecting a dimension too small would result in merging different RSNs and even noise. Here, the chosen dimension allowed to obtain RSNs comparable to those proposed in a recent consensus paper [27].

The interpretation of the results is also conditioned by the number of total observations studied. The number of animals was limited and the groups, both by age and sex, were not balanced. This is due to the fact that it is very difficult to carry out a longitudinal study where the same number of animals as at the beginning is maintained over time, due to different mortality rates across sexes and other factors.

The data acquisition and processing part is also a key part and influences the analysis and results directly. A recent consensus paper reported shared guidelines and suggestions on data acquisition and processing [27], which were followed in the present work. Another factor to note that directly affects the BOLD signal and must be taken into account in animal model fMRI studies is the choice of anesthetic. Previous studies uncovered the negative effect of the anaes-

thesia used on the BOLD signal, since it acts as a vasodilator, and the importance of keeping the animal within physiological limits for reliable data and interpretation [57, 32]. To this end, we followed the pipeline proposed in Grandjean, J. et al.[27].

Data preparation is an important step before processing begins and many intermediate preprocessing steps, such as labeling melodic components, are performed manually and can lead to incorrect data cleaning or misinterpretation. Also certain filtering parameters such as the spatial filtering kernel size (FWHM) are manually selected. A size of 6 mm has been chosen, although different larger dimensions have been tested and applying a larger size did not allow the identification of such localized networks. These values will depend on the study objective, but an incorrect choice can also lead to poor data cleaning. In this study, consistent RSNs have been found as reported in Grandjean, J. et al.[27].

7 Conclusions and future work

To conclude, we have reported a region-specific increase in functional connectivity in the ageing rat brain. Animal model is crucial for clinical applicability and translation to humans. Animal models make possible the longitudinal tracking of the subjects providing a richer information, difficult to obtain in clinical studies. In addition, since humans face a series of restrictions in time or certain healthy conditions, only animal model allows the optimization of sequences and research in advanced techniques in a preclinical environment. Its capability to extract information in a non-invasive manner makes magnetic resonance imaging an optimal tool for clinics.

As future steps, we plan to complement functional analysis with structural imaging or other metrics such as blood or histological parameters. Another study possibility is to combine the acquisition of sequences with behavioral and memory tests. Importantly, the results of this study will be presented as a poster at the next annual international congress ISMRM Iberian Chapter 2023.

8 Budget

1. **Personnel costs**
   This project has been carried out in collaboration with the Instituto de Neurociencias de Alicante, UMH-CSIC. The development of the project started in January 2023 and ended in June 2023, with a total of 880 hours, spread over 22 weeks, at a cost of 15 eur/h, amounting to a total of **13.200 eur/person**.

   A team of people is involved in the development of the project: the project manager, the MRI technician and the animal facility technician. The costs associated with these are not taken into account individually and are included in the costs associated with the MRI and the animal facility.

   The meetings on the evolution of the project with the supervisors from UPC and CSIC have been a total of approximately 10 hours each. Taking into account that the salary of these two people is 40 eur/h, it amounts to a total of **800 eur**.

2. **License costs**
   In the development of the project, open access software tools have been used (such as FSL or ANTs) and tools that have had 0 cost because they have a student license granted by the university, as is the case of Matlab.

3. **Material costs**

   (a) Animals: The price of a Wistar rat is 18.50 eur/animal. The associated cost with the animal service, maintenance and care is 1.54 eur/week. The purchase and acquisition of the sequences began approximately 90 weeks ago with the purchase of 40 rats (total of 740 eur). If only the maintenance of the animals used in this study is taken into account, the total cost is 2339 eur.

   (b) MRI facility. The acquisition of the MRI sequences includes the cost of the equipment, licenses and the technical staff involved. The acquisition costs 31 eur/h and an additional 10 eur/h for anesthetized animals. If there are a total of 38 sequences, of approximately 2 hours each, all of them under anesthesia, the total cost is 3116 eur.

   (c) Equipment. The project has been carried out using a computer with the following characteristics and price:

      i. PROCESSOR INTEL CORE i5-13600KF, 3.4GHZ, 24MB **285,2 eur**

      ii. Power Supply 750W **156,50 eur**

      iii. Tower box **45,37 eur**

      iv. Intel Asus PRIME B660M-K D4 board **100,70 eur**

      v. RAM DRAM Memory 32GB 3200Mhz **79,80 eur**

      vi. Cooler AM2/AM3 **66,90 eur**

      vii. Hard disk 1TB SSD **110,60 eur**

The total cost of the computer with IVA is 845,07 + 21% = 1.022,50 eur. Based on the duration of the project, the cost is estimated in proportion to the total cost of the project: **170.50 eur**.

8.1 Total associated costs

Taking into account the project development time, materials and equipment involved, the total cost of the project is 10000 eur. Table 3 shows a detail of total expenses.
These costs may vary depending on the type of animals to be used, the type of sequence to be acquired, the computer to be used and thus the time it takes to carry out the processing and analysis of the fMRI data.

Cost summary			
Personnel	13.200 eur	800 eur	-
License	Free	-	-
Materials	Computer	Animals	Facility
	170,50 eur	2.339 eur	3.116
Total			**19625,50 eur**

Table 3: Summary of project costs.

9 Project management

The Gantt diagram below illustrates the organisation that was followed on this project.

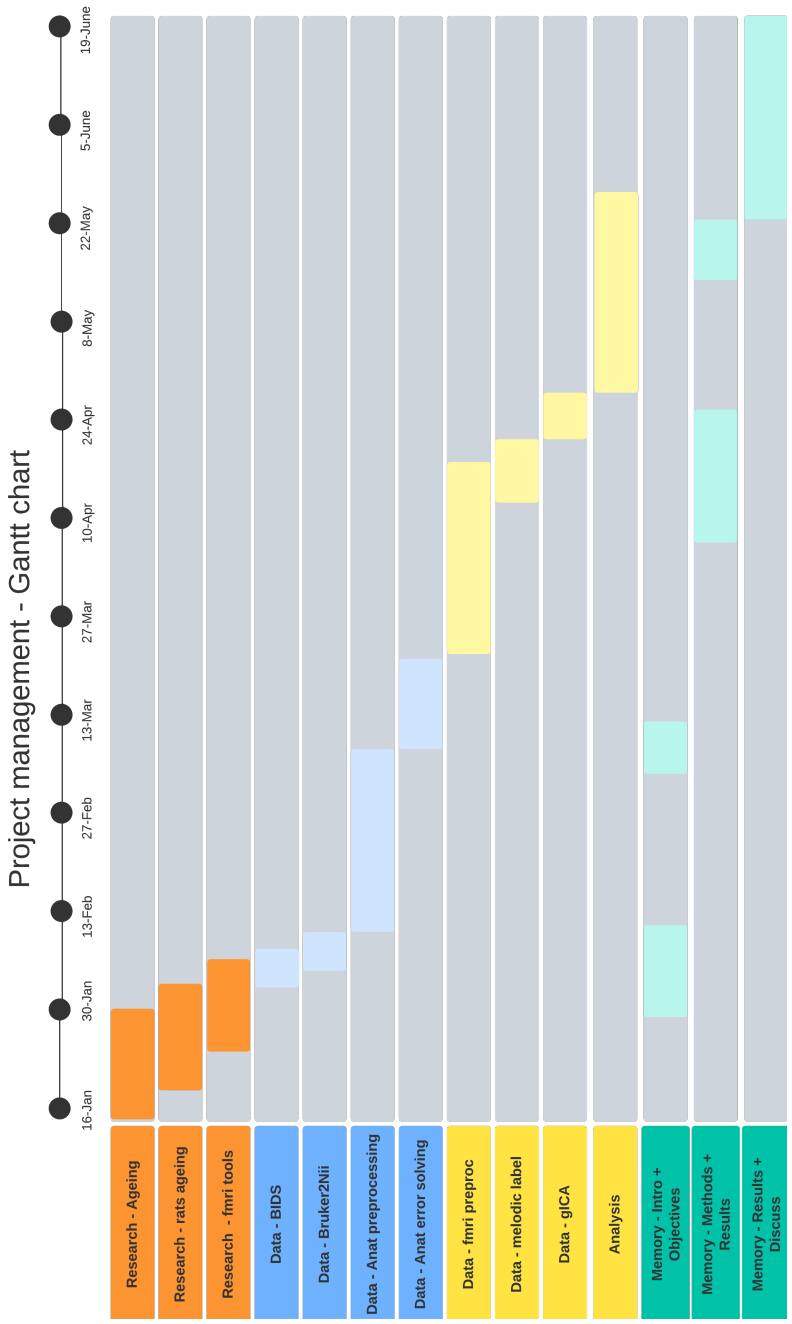

Figure 25: ***Gantt* diagram of the project**

10 Environmental impact analysis

This section evaluates the environmental impact of the development of this project.

The acquisition of images involves the MRI equipment and all the necessary additional software and hardware (coils, computers, anesthesia system, etc). The power consumption and heat dissipation is $\approx 7.5kW$ plus $\approx 7\ kW$ from the high power gradient amplifier. It is estimated that an average of 27.4 kWh is used during the sequence. This equipment was not purchased for the development of this project so its manufacturing impact will not be taken into account. In addition, a number of contaminated wastes are generated and have to be processed after use (needles, syringes, packaging, gauze, reagents, etc).
The use of isoflurane in combination with O_2 as an anesthetic and its release must also be taken into account. The use of anesthetic gases has a direct impact on greenhouse gas emissions and constitutes a high percentage of global emissions.

The maintenance of animals also has a large environmental impact but is necessary for their welfare. They must be kept in a room with constant temperature and relative humidity control. They must also follow light/dark cycles of 12 hours each. After completion of the study, the animals must be incinerated, generating emissions of various gases into the atmosphere.

The computer used to preprocess and analyze the data consumes between 200-230W at maximum power.

During the development of the project, the way to get to work has always been walking, thus reducing the emission of polluting fumes.

11 Acknowledgements

First of all, I would like to thank my supervisor Alejandro Bachiller for his guidance and dedication during these months of work. To my director, Silvia De Santis, for giving me the opportunity to learn great things by her side, for guiding me and welcoming me in her team.

This project would not have been possible without the Translational Imaging Biomarkers and the Plasticity of the Brain Networks laboratories. I would like to thank the whole team, especially to Dr. Santiago Canals and Dr. Silvia De Santis. Also, to my colleagues Antonio, Patricia, Andrés, Raquel and Ismael for their daily help.

Finally, thanks to my family and friends, especially *amics*, for their unconditional support, for never doubting me, for accompanying me during this master and pushing me to accomplish everything I set out to do. I carry with me great moments and people.

Bibliography

[1] Allen D. Elster., *T1 Relaxation: Definition. Questions and answers in MRI.*, https://mriquestions.com/what-is-t1.html

[2] Allen D. Elster., *T2 Relaxation: Definition. Questions and answers in MRI.*, https://mriquestions.com/what-is-t2.html

[3] Jenkinson, M., & Chappell, M., (2018) *Introduction to neuroimaging analysis.*, Oxford University Press,

[4] Damoiseaux J. S., (2017) *Effects of aging on functional and structural brain connectivity*, NeuroImage, 160, 32–40. https://doi.org/10.1016/j.neuroimage.2017.01.077

[5] Adriaanse, S. M., Binnewijzend, M. A., Ossenkoppele, R., Tijms, B. M., van der Flier, W. M., Koene, T., Smits, L. L., Wink, A. M., Scheltens, P., van Berckel, B. N., & Barkhof, F., (2014) *Widespread disruption of functional brain organization in early-onset Alzheimer's disease.*, PloS one, 9(7), e102995. https://doi.org/10.1371/journal.pone.0102995

[6] Fjell, A. M., Sneve, M. H., Grydeland, H., Storsve, A. B., & Walhovd, K. B., (2017) *The disconnected brain and executive function decline in aging.*, Cerebral cortex, 27(3), 2303-2317. https://doi.org/10.1093/cercor/bhw082

[7] Lee, M. S., (2021) *Methods of neuroimaging in depression: Applications to resting-state functional connectivity. In The Neuroscience of Depression (pp. 261-270). Academic Press.*

[8] Hafkemeijer, A., van der Grond, J., & Rombouts, S. A., (2012) *Imaging the default mode network in aging and dementia.*, Biochimica et Biophysica Acta (BBA)-Molecular Basis of Disease, 1822(3), 431-441.

[9] Hou, Y., Dan, X., Babbar, M., Wei, Y., Hasselbalch, S. G., Croteau, D. L., & Bohr, V. A. , (2019). Ageing as a risk factor for neurodegenerative disease. Nature reviews. Neurology, 15(10), 565–581. https://doi.org/10.1038/s41582-019-0244-7

[10] Joan, S., & Terry, L. J., (2010) *The basics of brain development*, Neuropsychol. Rev, 20, 327-348,

[11] Reddy, P. V., & Sastry, P. S., (1978) *Effect of undernutrition on the metabolism of phospholipids and gangliosides in developing rat brain.*, British Journal of Nutrition, 40(3), 403-411.

[12] Semple, Bridgette D and Blomgren, Klas and Gimlin, Kayleen and Ferriero, Donna M and Noble-Haeusslein, Linda J, (2013) *Brain development in rodents and humans: Identifying benchmarks of maturation and vulnerability to injury across species*, Elsevier, Progress in neurobiology, 106, 1–16

[13] Murman D. L., (2015) *The Impact of Age on Cognition.*, Seminars in hearing, 36(3), 111–121. https://doi.org/10.1055/s-0035-1555115

[14] Buckner, R. L., (2004) *Memory and executive function in aging and AD: multiple factors that cause decline and reserve factors that compensate*, Neuron, 44(1), 195-208.

[15] Park, Denise C, and Patricia Reuter-Lorenz., (2009) *"The adaptive brain: aging*

and neurocognitive scaffolding.", Annual review of psychology vol. 60 (2009): 173-96. doi:10.1146/annurev.psych.59.103006.093656

[16] De Godoy, L. L., Alves, C. A. P. F., Saavedra, J. S. M., Studart-Neto, A., Nitrini, R., da Costa Leite, C., & Bisdas, S., (2021) *Understanding brain resilience in superagers: a systematic review.*, Neuroradiology, 63, 663-683. https://doi.org/10.1007/s00234-020-02562-1

[17] Lee, B. H., Richard, J. E., de Leon, R. G., Yagi, S., & Galea, L. A, (2022) *Sex differences in cognition across aging. Sex Differences in Brain Function and Dysfunction*, 235-284.

[18] de Frias CM, Nilsson L-G, Herlitz A, (2006) *Sex differences in cognition are stable over a 10-year period in adulthood and old age.*, Neuropsychol Dev Cogn B Aging Neuropsychol Cogn 13(3–4):574–587. https://doi.org/10.1080/13825580600678418

[19] Voyer, D., Saint Aubin, J., Altman, K., & Gallant, G., (2021) *Sex differences in verbal working memory: A systematic review and meta-analysis.*, Psychological bulletin, 147(4), 352.

[20] Levine SC, Foley A, Lourenco S, Ehrlich S, Ratliff K, (2016) *Sex differences in spatial cognition: advancing the conversation.*, WIREs Cogn Sci 7(2):127–155. https://doi.org/10.1002/wcs.1380

[21] Sundermann, E. E., Tran, M., Maki, P. M., & Bondi, M. W., (2018) *Sex differences in the association between apolipoprotein E4 allele and Alzheimer's disease markers.*, Alzheimer's & dementia (Amsterdam, Netherlands), 10, 438–447, https://doi.org/10.1016/j.dadm.2018.06.004

[22] McCarrey AC, An Y, Kitner-Triolo MH, Ferrucci L, Resnick SM, (2016) *Sex differences in cognitive trajectories in clinically normal older adults.*, Psychol Aging 31(2):166. https://doi.org/10.1037/pag0000070

[23] Lee, B.H., Richard, J.E., de Leon, R.G., Yagi, S., Galea, L.A.M., (2022) *Sex Differences in Cognition Across Aging.*, In: Gibson, C., Galea, L.A.M. (eds) Sex Differences in Brain Function and Dysfunction. Current Topics in Behavioral Neurosciences, vol 62. Springer, Cham. https://doi.org/10.1007/7854_2022_309

[24] Fowler, C., Goerzen, D., Madularu, D., Devenyi, G. A., Chakravarty, M. M., & Near, J., (2022) *Longitudinal characterization of neuroanatomical changes in the Fischer 344 rat brain during normal aging and between sexes.*, Neurobiology of Aging, 109, 216-228. http://doi.org/10.1016/j.neurobiolaging.2021.10.003

[25] Bellantuono, I., de Cabo, R., Ehninger, D., Di Germanio, C., Lawrie, A., Miller, J., Mitchell, S. J., Navas-Enamorado, I., Potter, P. K., Tchkonia, T., Trejo, J. L., & Lamming, D. W., (2020) *A toolbox for the longitudinal assessment of healthspan in aging mice.*, Nature protocols, 15(2), 540–574. https://doi.org/10.1038/s41596-019-0256-1

[26] Desrosiers-Gregoire, G., Devenyi, G. A., Grandjean, J., & Chakravarty, M. M., (2022) *Rodent Automated Bold Improvement of EPI Sequences (RABIES): A standardized image processing and data quality platform for rodent fMRI*, bioRxiv, 2022-08.

[27] Grandjean, J., Desrosiers-Gregoire, G., Anckaerts, C., Angeles-Valdez, D., Ayad, F., Barrière, D. A., ... & Houwing, D. J., (2023) *A consensus protocol for functional connectivity anal-*

ysis in the rat brain., Nature neuroscience, 1-9.

[28] Wang, H. T., Meisler, S. L., Sharmarke, H., Clarke, N., Gensollen, N., Markiewicz, C. J., ... & Bellec, P., (2023) *A reproducible benchmark of resting-state fMRI denoising strategies using fMRIPrep and Nilearn.*, bioRxiv.

[29] Jenkinson, M., Bannister, P., Brady, J. M. and Smith, S. M., (2002) *Improved Optimisation for the Robust and Accurate Linear Registration and Motion Correction of Brain Images.*, NeuroImage, 17(2), 825-841.

[30] Bijsterbosch, J., Smith, S. M., & Beckmann, C. F., (2017) *An Introduction to Resting State Fmri Functional Connectivity*, Oxford University Press, USA

[31] Power, J. D., Barnes, K. A., Snyder, A. Z., Schlaggar, B. L., & Petersen, S. E., (2012) *Spurious but systematic correlations in functional connectivity MRI networks arise from subject motion.*, NeuroImage, 59(3), 2142-2154.

[32] Bajic, D., Craig, M. M., Mongerson, C. R. L., Borsook, D., & Becerra, L. , (2017) *Identifying Rodent Resting-State Brain Networks with Independent Component Analysis.*, Frontiers in neuroscience, 11, 685 https://doi.org/10.3389/fnins.2017.00685

[33] Ma, Z., Zhang, Q., Tu, W., & Zhang, N., (2022) *Gaining insight into the neural basis of resting-state fMRI signal.*, NeuroImage, 250, 118960. https://doi.org/10.1016/j.neuroimage.2022.118960

[34] Pérez Ramírez, MÚ., (2018) *Characterizing functional and structural brain alterations driven by chronic alcohol drinking: a resting-state fMRI connectivity and voxel-based morphometry analysis*,Universitat Politècnica de València. https://doi.org/10.4995/Thesis/10251/113164

[35] Beckmann, C. F., DeLuca, M., Devlin, J. T., & Smith, S. M., (2005) *Investigations into resting-state connectivity using independent component analysis.*, Philosophical transactions of the Royal Society of London. Series B, Biological sciences, 360(1457), 1001–1013. https://doi.org/10.1098/rstb.2005.1634

[36] Hyvarinen, A., (1997) *A family of fixed-point algorithms for independent component analysis.*, IEEE International Conference on Acoustics, Speech, and Signal Processing, 5, 3917-3920 vol.5.

[37] Griffanti, L., Douaud, G., Bijsterbosch, J., Evangelisti, S., Alfaro-Almagro, F., Glasser, M. F., ... & Smith, S. M., (2017) *Hand classification of fMRI ICA noise components.*, Neuroimage, 154, 188-205. https://doi.org/10.1016/j.neuroimage.2016.12.036

[38] Joel, S. E., Caffo, B. S., van Zijl, P. C., & Pekar, J. J., (2011) *On the relationship between seed-based and ICA-based measures of functional connectivity.*, Magnetic resonance in medicine, 66(3), 644–657, https://doi.org/10.1002/mrm.22818

[39] Nickerson, L. D., Smith, S. M., Öngür, D., & Beckmann, C. F., (2017) *Using dual regression to investigate network shape and amplitude in functional connectivity analyses.*, Frontiers in neuroscience, 11, 115.

[40] Crofts, A., Trotman-Lucas, M., Janus, J., Kelly, M., & Gibson, C. L., (2020) *A longitudi-*

nal, multi-parametric functional MRI study to determine age-related changes in the rodent brain., Neuroimage, 218, 116976.

[41] Straathof, M., Blezer, E. L., van Heijningen, C., Smeele, C. E., van der Toorn, A., Buitelaar, J., ... & Dijkhuizen, R. M., (2020) *Structural and functional MRI of altered brain development in a novel adolescent rat model of quinpirole-induced compulsive checking behavior.*, European Neuropsychopharmacology, 33, 58-70.

[42] Jobson, D. D., Hase, Y., Clarkson, A. N., & Kalaria, R. N., (2021) *The role of the medial prefrontal cortex in cognition, ageing and dementia.*, Brain communications, 3(3), fcab125.

[43] Bontempi, P., Podda, R., Daducci, A., Sonato, N., Fattoretti, P., Fiorini, S., ... & Marzola, P., (2021). *MRI characterization of rat brain aging at structural and functional level: Clues for translational applications.*, Experimental Gerontology, 152, 111432.

[44] Zhu, Z., Hakun, J. G., Johnson, N. F., & Gold, B. T., (2014). *Age-related increases in right frontal activation during task switching are mediated by reaction time and white matter microstructure.*, Neuroscience, 278, 51-61.

[45] Sengupta P., (2013) *The Laboratory Rat: Relating Its Age With Human's.*, International journal of preventive medicine, 4(6), 624–630.

[46] Mahoney, Jeannette R, and Joe Verghese., (2020) *Does Cognitive Impairment Influence Visual-Somatosensory Integration and Mobility in Older Adults?*, The journals of gerontology. Series A, Biological sciences and medical sciences vol. 75,3 : 581-588. doi:10.1093/gerona/glz117

[47] Ash, J. A., Lu, H., Taxier, L. R., Long, J. M., Yang, Y., Stein, E. A., & Rapp, P. R., (2016) *Functional connectivity with the retrosplenial cortex predicts cognitive aging in rats.*, Proceedings of the National Academy of Sciences, 113(43), 12286-12291.

[48] Li, P., Shan, H., Liang, S., Nie, B., Duan, S., Huang, Q., Zhang, T., Sun, X., Feng, T., Ma, L. & Shan, B., (2018) *Structural and functional brain network of human retrosplenial cortex.*, Neuroscience Letters, 674, 24-29.

[49] Buckner, Randy L., (2004) *"Memory and executive function in aging and AD: multiple factors that cause decline and reserve factors that compensate."*, Neuron vol. 44,1,(2004): 195-208. doi:10.1016/j.neuron.2004.09.006

[50] Slade, K., Plack, C. J., & Nuttall, H. E., (2020) *The effects of age-related hearing loss on the brain and cognitive function.*, Trends in Neurosciences, 43(10), 810-821.

[51] Ward, N. S., (2006) *Compensatory mechanisms in the aging motor system.*,Ageing research reviews, 5(3), 239-254.

[52] Wu, T., Zang, Y., Wang, L., Long, X., Li, K., & Chan, P., (2007) *Normal aging decreases regional homogeneity of the motor areas in the resting state.*, Neuroscience letters, 423(3), 189-193.

[53] Herlitz, A., Airaksinen, E., & Nordström, E., (1999) *Sex differences in episodic memory: the impact of verbal and visuospatial ability.*, Neuropsychology, 13(4), 590.

[54] Febo, M., Rani, A., Yegla, B., Barter, J., Kumar, A., Wolff, C.A., Esser, K. & Foster, T.C, (2020) *Longitudinal characterization and biomarkers of age and sex differences in the decline of spatial memory.*,Frontiers in Aging Neuroscience, 12, 34.

[55] Yagi, S., & Galea, L. A. M. , (2019). *Sex differences in hippocampal cognition and neurogenesis.*, Neuropsychopharmacology : official publication of the American College of Neuropsychopharmacology, 44(1), 200–213. https://doi.org/10.1038/s41386-018-0208-4

[56] Grissom, Elin M et al., (2013)*"Biological sex influences learning strategy preference and muscarinic receptor binding in specific brain regions of prepubertal rats."*, Hippocampus vol. 23,4 (2013): 313-22. doi:10.1002/hipo.22085

[57] Pan, W. J., Billings, J. C., Grooms, J. K., Shakil, S., & Keilholz, S. D., (2015) *Considerations for resting state functional MRI and functional connectivity studies in rodents.*, Frontiers in neuroscience, 9, 269. https://doi.org/10.3389/fnins.2015.00269

[58] McGeer, P. L., & McGeer, E. G., (2004) *Inflammation and the degenerative diseases of aging.*, Annals of the New York Academy of Sciences, 1035, 104–116. https://doi.org/10.1196/annals.1332.007

[59] Heneka, M. T., Carson, M. J., El Khoury, J., Landreth, G. E., Brosseron, F., Feinstein, D. L., Jacobs, A. H., Wyss-Coray, T., Vitorica, J., Ransohoff, R. M., Herrup, K., Frautschy, S. A., Finsen, B., Brown, G. C., Verkhratsky, A., Yamanaka, K., Koistinaho, J., Latz, E., Halle, A., Petzold, G. C., … Kummer, M. P., (2015) *Neuroinflammation in Alzheimer's disease.*, The Lancet. Neurology, 14(4), 388–405. https://doi.org/10.1016/S1474-4422(15)70016-5

[60] Liddelow, S. A., & Barres, B. A., (2017) *Reactive Astrocytes: Production, Function, and Therapeutic Potential.*, Immunity, 46(6), 957–967, https://doi.org/10.1016/j.immuni.2017.06.006

[61] Franceschi, C., Garagnani, P., Parini, P. et al., (2018) *Inflammaging: a new immune–metabolic viewpoint for age-related diseases.*,Nat Rev Endocrinol 14, 576–590 https://doi.org/10.1038/s41574-018-0059-4

[62] van der Meer, E., & van der Meer, J. W., (2011) *Inflammation and cardiovascular diseases: state of the art.*, Netherlands Heart Journal, 19(4), 166-169

[63] Chung, H. Y., Cesari, M., Anton, S., Marzetti, E., Giovannini, S., Seo, A. Y., Carter, C., Yu, B. P., & Leeuwenburgh, C., (2009) *Molecular inflammation: underpinnings of aging and age-related diseases.*, Ageing Research Reviews, 8(1), 18-30. https://doi.org/10.1016/j.arr.2008.07.002

[64] Hauser, S. L., & Oksenberg, J. R., (2006) *The neurobiology of multiple sclerosis: genes, inflammation, and neurodegeneration.*, Neuron, 52(1), 61–76, https://doi.org/10.1016/j.neuron.2006.09.011

[65] Ogawa, S., Lee, T. M., Kay, A. R., & Tank, D. W., (1990) *Brain magnetic resonance imaging with contrast dependent on blood oxygenation.*, Proceedings of the National Academy of Sciences of the United States of America, 87(24), 9868–9872. https://doi.org/10.1073/pnas.87.24.9868

[66] Fröhlich, F. , (2016) *Chapter 13—Imaging functional networks with MRI.*, Network Neuro-

science. Academic Press; San Diego, CA, USA, 177-185.

[67] Lu, H., Zou, Q., Gu, H., Raichle, M. E., Stein, E. A., & Yang, Y.(2012) *Rat brains also have a default mode network.*, Proceedings of the National Academy of Sciences of the United States of America, 109(10), 3979–3984. https://doi.org/10.1073/pnas.1200506109

[68] Park, D. C., Smith, A. D., Lautenschlager, G., Earles, J. L., Frieske, D., Zwahr, M., & Gaines, C. L.,(1996) *Mediators of long-term memory performance across the life span.*, Psychology and aging, 11(4), 621–637. https://doi.org/10.1037//0882-7974.11.4.621

[69] Broadhouse, K., (2020) *The physics of MRI and how we use it to reveal the mysteries of the mind.*, Frontiers for Young Minds, 7.

[70] Proal, E., Alvarez-Segura, M., de la Iglesia-Vayá, M., Martí-Bonmatí, L., Castellanos, F. X., & Spanish Resting State Network, (2011 *Actividad funcional cerebral en estado de reposo: redes en conexion* [*Functional cerebral activity in a state of rest: connectivity networks*], Revista de neurologia, 52 Suppl 1(0 1), S3–S10.

[71] Wu, T., Zang, Y., Wang, L., Long, X., Li, K., & Chan, P., (2007) *Normal aging decreases regional homogeneity of the motor areas in the resting state*, Neuroscience letters, 423(3), 189-193.